



Hippocampal and Cortical Pyramidal Neurons Swell in Parallel with Astrocytes during Acute Hypoosmolar Stress

Thomas R. Murphy^{1,2}, David Davila^{2,3}, Nicholas Cuvelier^{2,3}, Leslie R. Young^{2,3}, Kelli Lauderdale^{1,2}, Devin K. Binder^{1,2} and Todd A. Fiacco^{2,3*}

¹Division of Biomedical Sciences, School of Medicine, University of California, Riverside, Riverside, CA, United States,

²Center for Glial-Neuronal Interactions, University of California, Riverside, Riverside, CA, United States, ³Department of Cell Biology and Neuroscience, University of California, Riverside, Riverside, CA, United States

OPEN ACCESS

Edited by:

Keith Murai,
McGill University, Canada

Reviewed by:

Michelle Olsen,
University of Alabama at Birmingham,
United States
Yu-Feng Wang,
Harbin Medical University, China

*Correspondence:

Todd A. Fiacco
toddf@ucr.edu

Received: 29 June 2017

Accepted: 28 August 2017

Published: 20 September 2017

Citation:

Murphy TR, Davila D, Cuvelier N, Young LR, Lauderdale K, Binder DK and Fiacco TA (2017) Hippocampal and Cortical Pyramidal Neurons Swell in Parallel with Astrocytes during Acute Hypoosmolar Stress. *Front. Cell. Neurosci.* 11:275. doi: 10.3389/fncel.2017.00275

Normal nervous system function is critically dependent on the balance of water and ions in the extracellular space (ECS). Pathological reduction in brain interstitial osmolarity results in osmotically-driven flux of water into cells, causing cellular edema which reduces the ECS and increases neuronal excitability and risk of seizures. Astrocytes are widely considered to be particularly susceptible to cellular edema due to selective expression of the water channel aquaporin-4 (AQP4). The apparent resistance of pyramidal neurons to osmotic swelling has been attributed to lack of functional water channels. In this study we report rapid volume changes in CA1 pyramidal cells in hypoosmolar ACSF (hACSF) that are equivalent to volume changes in astrocytes across a variety of conditions. Astrocyte and neuronal swelling was significant within 1 min of exposure to 17 or 40% hACSF, was rapidly reversible upon return to normosmolar ACSF, and repeatable upon re-exposure to hACSF. Neuronal swelling was not an artifact of patch clamp, occurred deep in tissue, was similar at physiological vs. room temperature, and occurred in both juvenile and adult hippocampal slices. Neuronal swelling was neither inhibited by TTX, nor by antagonists of NMDA or AMPA receptors, suggesting that it was not occurring as a result of excitotoxicity. Surprisingly, genetic deletion of AQP4 did not inhibit, but rather augmented, astrocyte swelling in severe hypoosmolar conditions. Taken together, our results indicate that neurons are not osmoresistant as previously reported, and that osmotic swelling is driven by an AQP4-independent mechanism.

Keywords: hypoosmolar, cellular edema, AQP4, neuronal swelling, cell volume

INTRODUCTION

Acute reduction of plasma osmolarity in humans is a medical emergency, often resulting in seizures and sometimes coma or even death (Andrew, 1991; Castilla-Guerra et al., 2006). Such deleterious effects on the CNS can be attributed to the sudden change in osmotic pressure within the interstitial space of the brain, which causes cells to take on water leading to “cellular” or “cytotoxic” edema (Kimmelberg, 1995). Tissue swelling resulting from cellular edema has been observed in many studies examining the effect of hypoosmolar conditions on excitability (Andrew and MacVicar, 1994; Chebabo et al., 1995b; Kilb et al., 2006). Given that cell swelling shrinks the extracellular space

(ECS) and increases tissue resistance, hypoosmolar conditions amplify nonsynaptic excitability in neurons and increase susceptibility to seizure (Rosen and Andrew, 1990; Roper et al., 1992; Schwartzkroin et al., 1998; Lauderdale et al., 2015).

Most cellular edema in the brain is thought to be driven by water influx through aquaporin-4 (AQP4) channels, which are expressed primarily by astrocytes (Nagelhus et al., 2004). Knockout of AQP4 inhibits the tissue swelling normally associated with seizures (Binder et al., 2004), stroke (Katada et al., 2014), and other models of cytotoxic edema (Papadopoulos and Verkman, 2013). In normal physiology, AQP4 is important for water homeostasis in the brain, and appears to be required for the activity-dependent fluxes of water which occur alongside potassium uptake and buffering (Amiry-Moghaddam et al., 2003; Eid et al., 2005; Illarionova et al., 2010; Strohschein et al., 2011). Astrocytic swelling via AQP4-mediated water uptake is well-established as both a physiological and pathological phenomenon.

Neurons in most brain regions are thought to be resistant to volume changes except under pathological conditions. Pyramidal neurons in particular will rapidly swell in cases of oxygen-glucose deprivation (OGD) and excitotoxic damage (Choi, 1992; Andrew et al., 2007; Liang et al., 2007; Risher et al., 2009; Rungta et al., 2015), but appear very resistant to hypoosmolar swelling, an expected consequence of nonfunctional water channels (Gorelick et al., 2006; Andrew et al., 2007; Caspi et al., 2009). This has led to the conclusion that hypoosmolar swelling occurs mainly in glial cells (Andrew et al., 2007; Risher et al., 2009). However, this conclusion contradicts earlier reports of swelling under hypoosmolar stress in isolated pyramidal neurons in culture (Aitken et al., 1998; Somjen, 1999; Borgdorff et al., 2000). Furthermore, studies which have directly examined hypoosmolar swelling of pyramidal neurons or astrocytes (Andrew et al., 2007; Hirrlinger et al., 2008; Risher et al., 2009) have lacked temporal resolution below approximately 5 min. We have recently found that neuronal excitability increases significantly within 2 min of exposure to hypoosmolar ACSF (hACSF), suggesting that constriction of the ECS occurs rapidly during hACSF application (Lauderdale et al., 2015). Determining the precise contribution of cellular swelling and reduction of the ECS to rapid changes in neuronal excitability requires an equally rapid measurement of cell volume.

In the present study, we used confocal imaging to quantify stratum radiatum (s.r.) astrocyte and CA1 pyramidal neuron volume in acute mouse hippocampal slices during repeated 5–7 min hACSF applications, at 1-min resolution. Surprisingly, we found that CA1 neurons and s.r. astrocytes swell to the same extent and over a similar time course in both 17% and 40% hACSF. Neuronal swelling occurred across a variety of experimental conditions, suggesting that it is not an isolated phenomenon or attributable to one particular variable. Neuronal swelling did not differ between adult and juvenile animals, nor was it prevented by NMDA receptor antagonists, AMPA/Kainate receptor antagonists, TTX, or AQP4 deletion. Astrocyte swelling was also unaffected by AQP4 deletion in 17% hACSF and significantly augmented, rather than inhibited, in 40% hACSF. These data provide evidence that pyramidal neurons are not

osmoresistant and suggest that neurons and astrocytes may share a common, AQP4-independent swelling pathway in hypoosmolar conditions.

MATERIALS AND METHODS

All experiments were performed in accordance with National Institutes of Health guidelines for the care and use of laboratory animals, and approved by the Institutional Animal Care and Use Committee at the University of California, Riverside.

Slice Preparation in Juveniles

Hippocampal slices were prepared from juvenile (15–21 day old) C57Bl/6J mice as previously described (Xie et al., 2014). In some experiments, Thy1-enhanced green fluorescent protein (eGFP; Jackson Laboratories, Bar Harbor, ME, USA) or AQP4^{-/-} mice were utilized, both of which were on a C57Bl/6J background and exhibited no obvious phenotypic or behavioral differences from wild-type (Ma et al., 1997; Feng et al., 2000). Animals were deeply anesthetized under isoflurane and decapitated, and brains were quickly moved into ice-cold “slicing buffer” containing (in mM): 125 NaCl, 2.5 KCl, 3.8 MgCl₂, 1.25 NaH₂PO₄, 26 NaHCO₃, 25 glucose and 1.3 ascorbic acid, bubbled continuously with carbogen (95% O₂/5% CO₂). Parasagittal hippocampal slices (350 μm thick) were prepared using a Leica VT1200S vibratome (Leica, Nussloch, Germany) and transferred to a recovery chamber containing standard artificial cerebrospinal fluid (ACSF), which was composed of (in mM): 125 mM NaCl, 2.5 KCl, 2.5 CaCl₂, 1.3 mM MgCl₂, 1.25 NaH₂PO₄, 26 NaHCO₃ and 15 glucose, bubbled continuously with carbogen (~299–303 mOsm). Slices were incubated in ACSF at 36°C for 45 min, then allowed to cool to room temperature for a minimum of 15 min before being transferred to a recording chamber for experiments.

In some cases, sulforhodamine-101 (SR-101; Sigma-Aldrich, St. Louis, MO, USA) was used during incubation to selectively stain astrocytes (Schnell et al., 2015). Incubation was adjusted as follows (Xie et al., 2014): After preparation, slices were transferred to a recovery chamber containing 1 μM SR-101, dissolved in a modified ACSF composed of (in mM): 125 NaCl, 2.5 KCl, 0.5 CaCl₂, 6 MgCl₂, 1.25 NaH₂PO₄, 26 NaHCO₃, 15 glucose and 1.3 ascorbic acid, bubbled continuously with carbogen, and incubated at 36°C for 25–35 min. Slices were subsequently transferred to the same modified ACSF without SR-101 for 10 more minutes at 36°C. Finally, slices were allowed to cool to room temperature for 15 min before being transferred to ACSF. Slices were equilibrated in ACSF for at least 15 min prior to use. For experiments performed at physiological temperature, slices were kept at 36°C.

The use of SR-101 has recently been called into question, in part due to its reported potentiation of NMDA receptor activity and tissue excitability (Kang et al., 2010; Rasmussen et al., 2016). However, modified ACSF used during SR-101 incubation included 6 mM Mg²⁺, and TTX, NBQX, and AP5 had no appreciable effects on astrocyte or neuronal volume changes. SR-101 labeling specificity is another, more recent concern (Hill and Grutzendler, 2014; Hagos and Hülsmann, 2016).

Based on patch-clamp analysis of SR-101 labeled cells, we have observed that ~87% of SR-101-labeled cells are astrocytes based on their electrophysiological parameters, indicating that SR-101 is highly reliable as an astrocyte marker for our purposes.

Slice Preparation in Adults

Adult (10–15 week old) hippocampal slices were prepared from C57Bl/6J or Thy1-eGFP mice as previously described (Lauderdale et al., 2015). Adult slicing buffer (ASB) contained (in mM): 87 NaCl, 75 sucrose, 2.5 KCl, 0.5 CaCl₂, 7 MgCl₂, 1.25 NaH₂PO₄, 25 NaHCO₃, 10 glucose, 1.3 ascorbic acid, 2 pyruvate, 3.5 MOPS and 100 μM kynurenic acid, bubbled continuously with carbogen, and was partially frozen to form an icy “slush”. Slices were prepared as described above, and transferred to a recovery chamber containing carbogen-bubbled ASB at 36°C for 45 min. Following incubation, slices were allowed to cool to room temperature for 15 min before being transferred to standard ACSF, where they equilibrated for a minimum of 20 min before being used for experiments.

The SR-101 protocol was adapted for use in adults by adding SR-101 to the ASB which was similar in composition to the modified ACSF normally used for SR-101 loading. For unknown reasons, adult astrocytes proved far more resistant to SR-101 loading than did juvenile astrocytes, and required additional modifications to our labeling protocol. We found that a 45-min incubation in 2–4 μM SR-101 labeled adult astrocytes to a similar degree and depth as juvenile astrocytes, with limited background staining. Slices were cooled to room temperature for 15 min in SR-101-free ASB after incubation, and then transferred to standard ACSF as above.

Solutions and Drugs

“Normosmolar ACSF” (nACSF, ~298 mOsm), consisting of standard ACSF without MgCl₂, was used for baseline recordings and wash periods. Seventeen or 40% “hypoosmolar ACSF” (hACSF) was prepared by using deionized water to dilute nACSF by 10% (final osmolarity: ~270 mOsm), 17% (final osmolarity: ~250 mOsm) or 40% (final osmolarity: ~180 mOsm). These percent reductions in osmolarity have been generally described as “mild” to “modest” (<20% hypoosmolarity; Azouz et al., 1997; Thrane et al., 2011; Anderova et al., 2014) or “moderate” to “severe” (>30% hypoosmolarity; Kimelberg, 2004; Kimelberg et al., 2006; Anderova et al., 2014), and were chosen based on those often used in previous studies which have ranged anywhere from 5% to 65% (Chebabo et al., 1995b; Darby et al., 2003; Kimelberg, 2004; Kilb et al., 2006; Andrew et al., 2007; Fiacco et al., 2007; Haskew-Layton et al., 2008; Hirrlinger et al., 2008; Wurm et al., 2010; Thrane et al., 2011; Lauderdale et al., 2015). Unless otherwise indicated, “experimental” ACSF solutions (nACSF and hACSF) contained 1 μM TTX (Cayman Chemical, Ann Arbor, MI, USA) to block voltage-gated Na⁺ channels, and 10 μM NBQX (Alomone Labs, Jerusalem, Israel) to block AMPA/Kainate receptors (Lauderdale et al., 2015). In some experiments, 50 μM AP5 (an NMDA-receptor antagonist; Abcam, Cambridge, MA, USA) or 6 mM Mg²⁺ (to maximize block of NMDA receptors in the slice;

Dissing-Olesen et al., 2014) were also added to the experimental solutions.

A number of experiments were performed using more “physiological” antagonist-free solutions, which were based on standard (1.3 mM Mg²⁺) ACSF and contained no TTX or NBQX. In these experiments, standard ACSF was used in place of nACSF for baseline and wash periods, and diluted by 17% or 40% to generate the respective hACSF doses.

Patch-Clamp of Neurons and Astrocytes

Hippocampal slices were transferred to a recording chamber and continuously superfused with room-temperature, oxygenated ACSF. For experiments at physiological temperature, recording chamber and perfusion solution temperatures were maintained at 36°C using a Warner Instruments TC-344B Dual Channel Heater Controller (Warner Instruments, Hamden, CT, USA). Slices were visualized using an Olympus BX61 WI upright microscope equipped with UMPLFLN 10× (N.A. 0.3) and LUMPlanFl 60× (N.A. 0.9) water-immersion objectives and DIC optics (Olympus America, Center Valley, PA, USA). CA1 pyramidal neurons and passive stratum radiatum (s.r.) astrocytes were patch clamped in order to load them with fluorescent indicator dyes for volume measurements in our initial experiments. Whole-cell patch clamp was performed using a Multiclamp 700B amplifier and Digidata 1550 digitizer, controlled through pClamp v.10.4 and Multiclamp commander software (Molecular Devices, Sunnyvale, CA, USA). Patch pipettes were pulled from borosilicate glass using a Narishige PC-10 vertical micropipette puller (Narishige, Tokyo, Japan). Neuronal patch pipettes had a resistance of 3.8–5.3 MΩ when filled with an internal solution containing (in mM): 140 K-gluconate, 4 MgCl₂, 0.4 EGTA, 4 Mg-ATP, 0.2 Na-GTP, 10 HEPES, and 10 phosphocreatine, pH 7.3 with KOH. For dye loading, neuronal patch pipettes also contained the fluorophores Alexa 488 hydrazide (100–200 μM) or Alexa 594 hydrazide (200 μM; Thermo Fisher Scientific, Waltham, MA, USA). Astrocyte patch pipettes had resistances of 4.2–8.9 MΩ when filled with an internal solution containing (in mM): 130 K-gluconate, 4 MgCl₂, 10 HEPES, 10 glucose, 1.185 Mg-ATP, 10.55 phosphocreatine and 0.1315 mg/ml creatine phosphokinase, pH 7.3 by KOH. Astrocyte pipettes also contained 100–200 μM Alexa Fluor 488 dextran or Oregon Green 488 dextran (Thermo Fisher Scientific), both 10 kDa in size to prevent dye spread into neighboring astrocytes via gap junctions.

Neurons and astrocytes were identified first by location and morphology under DIC optics, and confirmed by their electrophysiological properties, as routinely performed by our group (Sun et al., 2014). Pyramidal neuron resting V_m was -60.1 ± 0.7 mV ($n = 30$) and exhibited characteristic voltage-gated Na⁺ and K⁺ currents in response to a voltage step protocol. Astrocytes were identified based on a characteristically low input resistance, low resting membrane potential (-78.0 ± 1.2 mV; $n = 15$) and passive membrane properties. Astrocytes and neurons were voltage-clamped to -90 or -70 mV, respectively, for no more than 5 min to allow for dye diffusion into the cytoplasm (with rare exceptions for dextran-loading of

astrocytes, which sometimes required up to 8 min). In the interest of limiting the amount of cytoplasm dialyzed by the internal solution, this time was kept to a minimum with occasional, quick confocal scans to check cell brightness. Once dye loading was deemed sufficient for imaging, the pipette was gently withdrawn. A smooth, stable “off-cell” and formation of a $> 1 \text{ G}\Omega$ seal during pipette removal was considered an indicator that the cell was not damaged during withdrawal of the patch pipette. All patch clamped cells were allowed to recover for at least 10 min before further use. In later experiments, patch clamp was mostly supplanted by bulk loading astrocytes with SR-101 dye (see above), and by using neurons from the Tg(Thy1-EGFP)Mjrs/J (Thy1-GFP-M, stock #7788) or B6;CBA-Tg(Thy1-EGFP)Sjrs/NdivJ (Thy1-GFP-S, stock #11070) mouse lines, which express eGFP under the neuronal Thy1 promoter in some pyramidal neuron populations (Feng et al., 2000). In these instances, cells were chosen based on their depth in the tissue, lack of obvious morphological abnormalities, and their visibility under our standard imaging settings (see below).

Confocal Imaging Settings and Experimental Design

Alexa Fluor 488 dextran, Oregon green 488 dextran, Alexa Fluor 488, and eGFP were excited using a 488 nm argon laser (Melles Griot, Carlsbad, CA, USA) and detected with a 503–548 nm bandpass filter, controlled by Olympus Fluoview 1000 software. Laser power was generally held at $\leq 2.0\%$, well below the level needed to induce photobleaching ($> 50\%$). Pixel dwell time was 8 $\mu\text{s}/\text{pixel}$ for astrocytes (which often required extra exposure time due to limited dextran loading) and 4 $\mu\text{s}/\text{pixel}$ for neurons. Alexa Fluor 594 and SR-101 were excited using a 559 nm semiconductor laser and detected using a 624–724 nm bandpass filter. Pixel dwell times were kept the same as above for consistency. Laser power $\leq 1.5\%$ was sufficient to detect SR-101 labeled astrocytes and Alexa Fluor 594 labeled neurons. To strike an appropriate balance between image resolution and brightness, confocal aperture size was set to 300 μm and PMT voltage $\sim 830 \text{ V}$ across all experiments.

In one experiment, Thy1-eGFP neurons were examined much deeper within the slice ($> 60 \mu\text{m}$ below slice surface) and were in many cases impossible to image using our standard settings. Instead, laser power was increased to 10% and pixel dwell time to 8 $\mu\text{s}/\text{pixel}$, increasing acquisition time per image stack ($\sim 15\text{--}30 \text{ s}$) but significantly boosting cell visibility. We observed no deleterious effects on cell health resulting from the increase in laser power or exposure time.

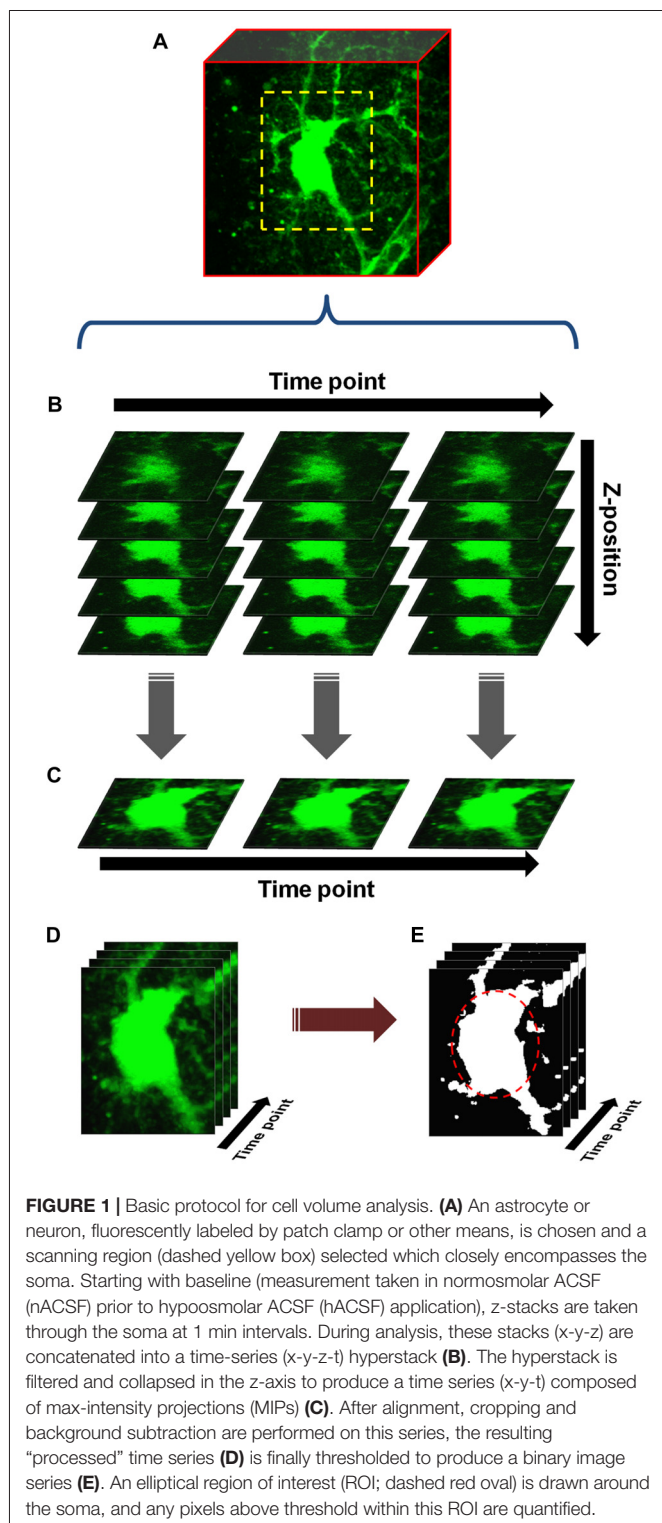
All experiments started in standard ACSF. Where applicable, standard ACSF was replaced by nACSF following patch pipette removal or identification of the cell to be imaged, and allowed to wash in for 10 min prior to imaging. Imaging consisted of confocal z-stacks taken through the cell soma, beginning with a single “baseline” stack. As observed by other groups (Hirrlinger et al., 2008; Risher et al., 2009), we found that single images were insufficient for gathering the full extent of the cell body in the x-y plane (which is necessary for soma area

measurements, our proxy for cell volume), and were particularly vulnerable to swelling-induced z-shifts across time points. We instead opted for rapid z-stacks through the soma, at 1.0 μm intervals and a zoom level of $3.5\times$ (0.118 $\mu\text{m}/\text{pixel}$). X, Y and Z-shifts were compensated using quick confocal scans to check cell position, and adjusting X-Y position and Z-scan upper/lower limits accordingly before acquiring each stack. To increase scan speed, the “clip scan” function was used to crop the scan window close around the soma, reducing acquisition time to $\sim 15 \text{ s}$ per stack. These settings allowed us to obtain full z-stacks through the cell soma at 1-min intervals. For simplicity, a z-stack encompassing the cell soma will hereafter be referred to as a “stack”.

After a baseline stack was obtained, hACSF was applied for 5 min and a single stack was acquired at the end of each minute. hACSF was then “washed out” by re-application of normosmolar ACSF (either nACSF or standard ACSF) for 5 min, at the end of which an additional stack was acquired. This sequence was repeated an additional two times to determine repeatability of effects on cell volume. Each subsequent hACSF application and wash period was lengthened by 1 min (after which an additional stack was acquired), due to our observations (unpublished) that neuronal slow inward currents (SICs) evoked in these conditions were more “spread out” during subsequent hACSF applications.

Volume Analysis Protocol

Analysis of neuron and astrocyte volume was performed using the FIJI distribution of ImageJ as previously described (Schindelin et al., 2012; Lauderdale et al., 2015). Our basic analysis protocol is depicted in **Figure 1**. First, z-shifts across time points were corrected by choosing a common landmark and matching its slice number across all stacks. Stacks were then concatenated into an x-y-z-t hyperstack (**Figure 1B**), and filtered to remove noise (median filter, 2 pixel diameter). A max-intensity z-projection (MIP) was made through this hyperstack, producing a 2D time series (**Figure 1C**), in which each frame was a MIP showing the full x-y extent of the soma at a given time point. X-Y shifts over time were corrected using the “Linear Stack Alignment with SIFT” plugin (followed by cropping, to remove the blank areas left by image alignment), and background subtraction was performed using FIJI’s background subtraction tool (radius 50 pixels, sliding paraboloid method). The resultant time series (**Figure 1D**) was then binarized using the “mean” thresholding algorithm (**Figure 1E**) and an elliptical ROI was drawn to narrowly encompass the soma across all time points in the series (dashed red circle, **Figure 1E**). Area above threshold within this ROI (a measure of soma area) was used as a proxy for soma volume. Volume changes at a given time point are reported as percent change from baseline soma volume. Some experiments also include the “average percent change” from baseline over three hACSF applications. In these cases, percent change in the 2nd and 3rd hACSF periods is calculated based on the preceding nACSF wash instead of the original baseline, providing a more accurate measure of acute, relative volume changes during hACSF application. Representative images, unless otherwise noted, depict the thresholded images used for analysis.



In an effort to better analyze neurons from “deep” tissue (which were not amenable to our standard analysis protocol due to poor resolution of cell borders), we employed a simplified version of the microspectrofluorimetric method of measuring volume (Crowe et al., 1995). This method does not rely on

cell borders but rather on fluorescence intensity, allowing for estimation of cell volume changes using a region of interest (ROI) placed in the cell center. In brief, this method assumes a fixed number of fluorescent molecules within a cell, and therefore that any changes in cell water content (i.e., cell swelling or shrinking) will alter their concentration. As dye becomes less concentrated, fluorescence (F) should decrease linearly, and vice versa. Cell volume changes are thus inversely related to changes in cell fluorescence ($\frac{F_t}{F_0}$), where F_t = cell fluorescence at the time point of interest and F_0 = baseline cell fluorescence, and can be roughly calculated as the inverse of the fluorescence ratio ($\frac{F_0}{F_t}$). Fluorescence ratios were determined by drawing an ROI $5 \mu\text{m} \times 5 \mu\text{m}$ wide over the center of a given cell in a processed MIP time series stack (just prior to thresholding) and measuring average intensity in this region at each time point.

Statistical Analysis

Statistical analysis was performed with SPSS Statistics 22 or 23 software (IBM Corporation, Armonk, NY, USA). Mixed-design ANOVA was used for all tests to determine changes from baseline over time (within-subject factor) and between treatments, genotypes or cell types (between-subject factor). Outliers were in rare cases excluded from analysis, and only one outlier was removed from any particular group. A cell identified as an outlier was considered for removal only if: (a) its removal improved the reliability of ANOVA results (making group N more equal, reducing normality or homogeneity of variance violations, etc); and (b) measurement errors were clearly responsible for the aberrant data. Significant within-subject effects were investigated further by pairwise comparisons of each time point group to baseline. Multiple comparisons between time points were adjusted performed using the Holm-Bonferroni method, a stepwise procedure with the same assumptions as the Bonferroni correction but substantially more power for larger numbers of comparisons. Significant between-subject effects were further investigated by Student’s t -test or (if three or more groups) using pairwise comparisons with Bonferroni correction. Significant interactions were investigated in two steps. First, between-group simple effects were tested at each time point using Student’s t -test (for two groups) or one-way ANOVA followed by Tukey’s HSD *post hoc* tests (for three or more groups). In the case of normality or homoscedasticity violations, appropriate alternatives were chosen (e.g., Welch t -test or Mann-Whitney U). Second, within-subjects simple effects were determined by splitting the file by group and running each as an individual one-way repeated measures ANOVA, with Holm-Bonferroni *post hoc* tests as above. This “split-file” method has the effect of splitting the error terms by group and was deemed to be more accurate than obtaining simple main effects within the original mixed ANOVA, as the latter uses a pooled error in its calculations. $N = 7\text{--}10$ cells per group (after outlier removal) for all experiments, unless indicated otherwise. Significant differences are reported at the $p < 0.05$ (*), $p < 0.01$ (**), and $p < 0.001$ (***) levels.

RESULTS

In a previous study, we found heightened neuronal excitability within 1 min of exposing hippocampal slices to 17% or 40% hACSF (Lauderdale et al., 2015). The primary focus of the current study was to examine the volume changes exhibited by neural cells over this time period. While it has been reported that hypoosmolar volume changes are mainly limited to astrocytes (Andrew et al., 2007; Caspi et al., 2009; Risher et al., 2009), conflicting reports suggest this may not always be the case (Aitken et al., 1998; Borgdorff et al., 2000; Boss et al., 2013). Therefore, we chose to examine volume responses of stratum radiatum (s.r.) astrocytes as well as CA1 pyramidal neurons, using hypoosmolar solutions (denoted hACSF for simplicity) made by 17% or 40% dilution of standard ACSF with distilled water, and including TTX (1 μ M), NBQX (10 μ M) and 0 mM Mg^{2+} by default. These conditions were chosen to match our previous work demonstrating significant stimulation of NMDA receptor currents by hACSF in CA1 pyramidal neurons (Lauderdale et al., 2015). The use of TTX to block neuronal firing also reduced the likelihood of spreading depression, a wave of depolarization and subsequent synaptic silencing which has sometimes been observed in hypoosmolar conditions (Chebabo et al., 1995a). Normosmolar ACSF (nACSF), used during the baseline and wash periods, was not diluted but otherwise identical in composition to the above.

Astrocytes and Neurons Swell to Approximately Equal Volumes in Hypoosmolar ACSF

We first examined the volume responses of CA1 pyramidal neurons and s.r. astrocytes to repeated applications of 17% and 40% hACSF (Figure 2). Neurons (Figures 2A–D) and astrocytes (Figures 2E,F) were initially labeled by patch-clamp dialysis of the fluorescent indicators Alexa Fluor 568 hydrazide or fluorescein dextran, respectively, and imaged using confocal microscopy (see “Materials and Methods” Section). As in our previous study, image stacks through cell somata were collected at 1-min intervals starting with a baseline in nACSF (Figures 2A1,E1), and proceeding through 5 min of hACSF (Figures 2A2,E2), with a final image stack acquired after a 5 min “wash” in nACSF (Figures 2A3,E3). Stacks were post-processed and thresholded (Figure 2B) to quantify percent change from baseline at each time point (Figure 1; also see “Materials and Methods” Section). In contrast to some previous studies in which neuronal volume was insensitive to hypoosmolar shifts (Andrew et al., 2007; Caspi et al., 2009), we found that neurons rapidly swelled in response to both 17% and 40% hACSF, and this swelling was similar in magnitude and time course to volume changes in astrocytes (Figures 2A–D). Neuronal soma area significantly increased above baseline within 1 min in 17% ($2.04 \pm 0.33\%$, $p < 0.001$) or 40% ($2.09 \pm 0.72\%$, $p = 0.044$) hACSF, and continued to gradually increase to a maximum of $4.72 \pm 0.41\%$ in 17% hACSF and $10.51 \pm 0.93\%$ in 40% hACSF (Figure 2D). Overlays of baseline

and 5 min 40% hACSF time points (Figure 2C2) facilitate visualization of these volume increases as magenta expansions along the outer border of the cell. Neurons largely recovered to baseline volume after a 5 min wash period in nACSF ($1.27 \pm 0.39\%$ above baseline in 17%, $2.70 \pm 0.92\%$ in 40% hACSF, $p < 0.05$ each), as shown in Figure 2C3 overlays. These data bore a remarkable similarity to our observations of s.r. astrocytes in the same conditions (Figures 2E,F). As reported in Lauderdale et al. (2015), astrocytes also rapidly swelled in both concentrations of hACSF within the first minute ($p < 0.01$) and in a dose-dependent manner. Unlike neurons, astrocytes fully recovered to baseline volume upon return to nACSF for 5 min.

Swelling of both neurons and astrocytes was repeatable upon additional applications of 40% or 17% hACSF (Figure 2G; Supplementary Movie S1). No neuronal swelling was detected in the absence of hACSF (Figure 2G; $n = 6$). No significant interaction was found between cell type and time point (40% hACSF, $F_{(2,66,34,64)} = 1.12$, $p = 0.351$; 17% hACSF, $F_{(4,11,65,73)} = 1.12$, $p = 0.355$), suggesting largely identical swelling characteristics between the two cell types.

Neuronal Health Is Unlikely to be a Contributing Factor to hACSF-Induced Swelling

We began to examine the key differences in experimental protocol between our study and previous work, to determine if an unforeseen factor was responsible for (or contributing to) the neuronal swelling observed in our conditions.

Although we had no reason to suspect damage to the cell using whole-cell patch clamp approaches (see “Materials and Methods” Section), we considered the possibility that the simple act of patch clamping neurons may make them more susceptible to hACSF-induced swelling. We tested this by using hippocampal slices from transgenic Thy1-eGFP mice (Feng et al., 2000). These mice express eGFP in a sparse, random population of pyramidal neurons (Figure 3A), making them ideal for isolating a single neuron in the densely packed pyramidal layer of the hippocampal CA1 region (Andrew et al., 2007). Neurons expressing eGFP were bright and easily identified at our standard imaging depth of 30–40 μ m (Figure 3B1, left) and once again exhibited distinct volume changes upon exposure to 40% hACSF (Figure 3B2, right). Compared to patch-loaded neurons, Thy1-eGFP neurons at this depth showed no significant difference in swelling responses to 40% hACSF ($F_{(1,16)} = 0.98$, $p = 0.336$; Figure 3C) or 17% hACSF ($F_{(1,16)} = 1.36$, $p = 0.26$; data not shown).

With a moderate increase in laser power (10% of maximum), we were able to extend our imaging range to ~65–90 μ m below the slice surface (Figures 4A1,A2), considerably deeper than what was feasible by patch clamp. Deeper neurons initially appeared to be more resistant to volume change in 40% hACSF (Figure 4B), with an average relative increase of only $4.22 \pm 0.39\%$ after 5 min in hACSF (Figure 4B, inset). This apparent reduction in osmosensitivity, however, was most likely a detection issue. Resolution of the boundary of these cells

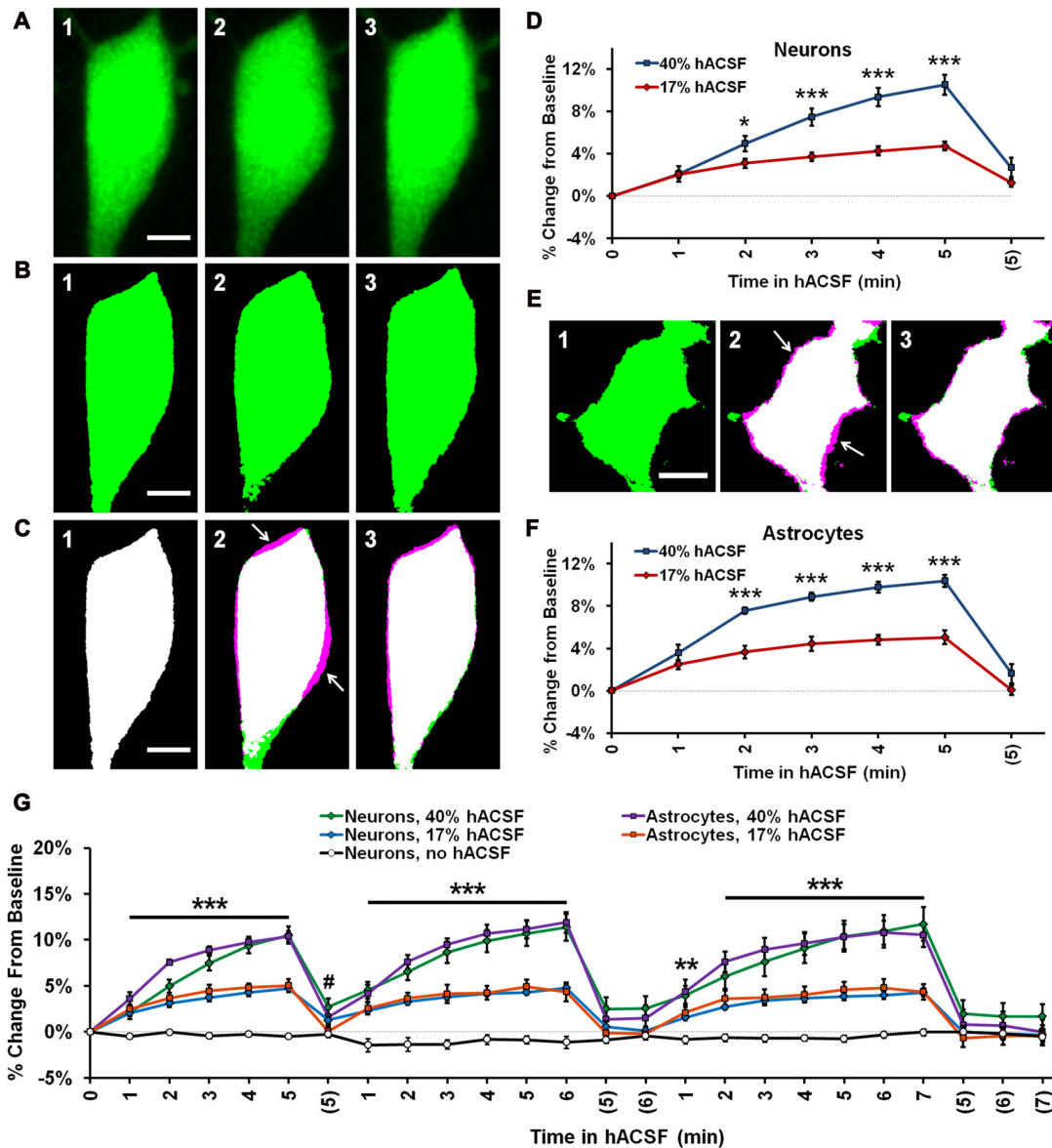


FIGURE 2 | Neurons and astrocytes both swell in hypoosmolar conditions. **(A)** Representative MIPs of a CA1 pyramidal neuron loaded with Alexa Fluor 488 dye via patch clamp, depicting soma volume at baseline **(A1)**, followed by 5 min in 40% hACSF **(A2)**, and a subsequent 5 min wash period in nACSF **(A3)**. Swelling of the soma during hACSF application is readily apparent in **(A2)**. **(B1–B3)** Time points in **(A1–A3)** are processed and binarized (see **Figure 1**) to allow measurement of soma area. Images are pseudocolored green for easier comparison with **(A)**. **(C)** Each thresholded image in **(B)** is pseudocolored magenta and overlaid with green baseline image from **(B)** to reveal regions of soma expansion during 40% hACSF, which recover to near basal levels upon return to nACSF (magenta highlights, indicated by white arrows). Scale bars = 5 μ m. **(D)** Quantification of neuronal soma volume as a percent change from baseline area in 17% and 40% hACSF conditions over a single 5-min application, followed by a 5 min wash period denoted with (5). Time points 0, 5 and (5) correspond to images in **(A1–A3)** respectively. **(E)** Representative thresholded images of an astrocyte loaded with Alexa Fluor 488 dextran (10,000 MW) at baseline **(E1)**, after 5 min in 40% hACSF **(E2)**, and after a 5 min wash in nACSF **(E3)**. As in **(A)**, images in **(E2,E3)** have been overlaid with the baseline image to illustrate changes in cell volume (white arrows). Scale bar = 5 μ m. **(F)** Quantification of astrocyte soma volume as a percent change from baseline area in 17% and 40% hACSF conditions. * $p < 0.05$ and *** $p < 0.001$ for 17% vs. 40% at each time point in **(D,F)**. All time points for both 17% and 40% hACSF were significantly elevated over baseline. **(G)** Expanded time course showing neuron and astrocyte volume changes over multiple re-applications of 40% or 17% hACSF. Neuron volume in control conditions (“no hACSF”, black line) is included for comparison. *** $p < 0.001$, ** $p < 0.01$ (both cell types) and # $p < 0.05$ (astrocytes only), percent change vs. 0% (baseline). $N = 7–9$ cells per hACSF group and six cells for control.

was poor, which tended to be exacerbated by the thresholding step of our analysis. For shallower neurons, both the original image (**Figure 4C1**) and its thresholded version (indicated by

magenta outlines on **Figure 4C1**) tended to reflect similar cell borders. By contrast, much of the visible cell border in deeper neurons fell below threshold, and the final thresholded

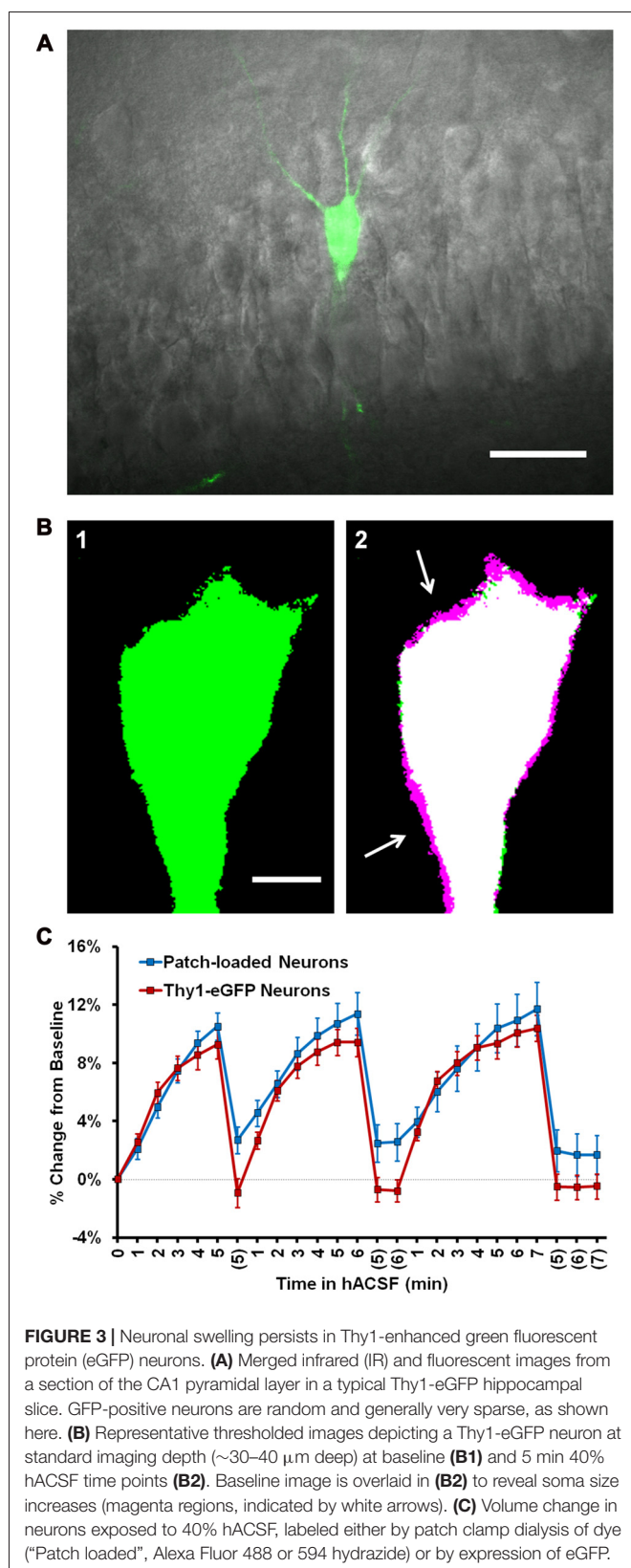
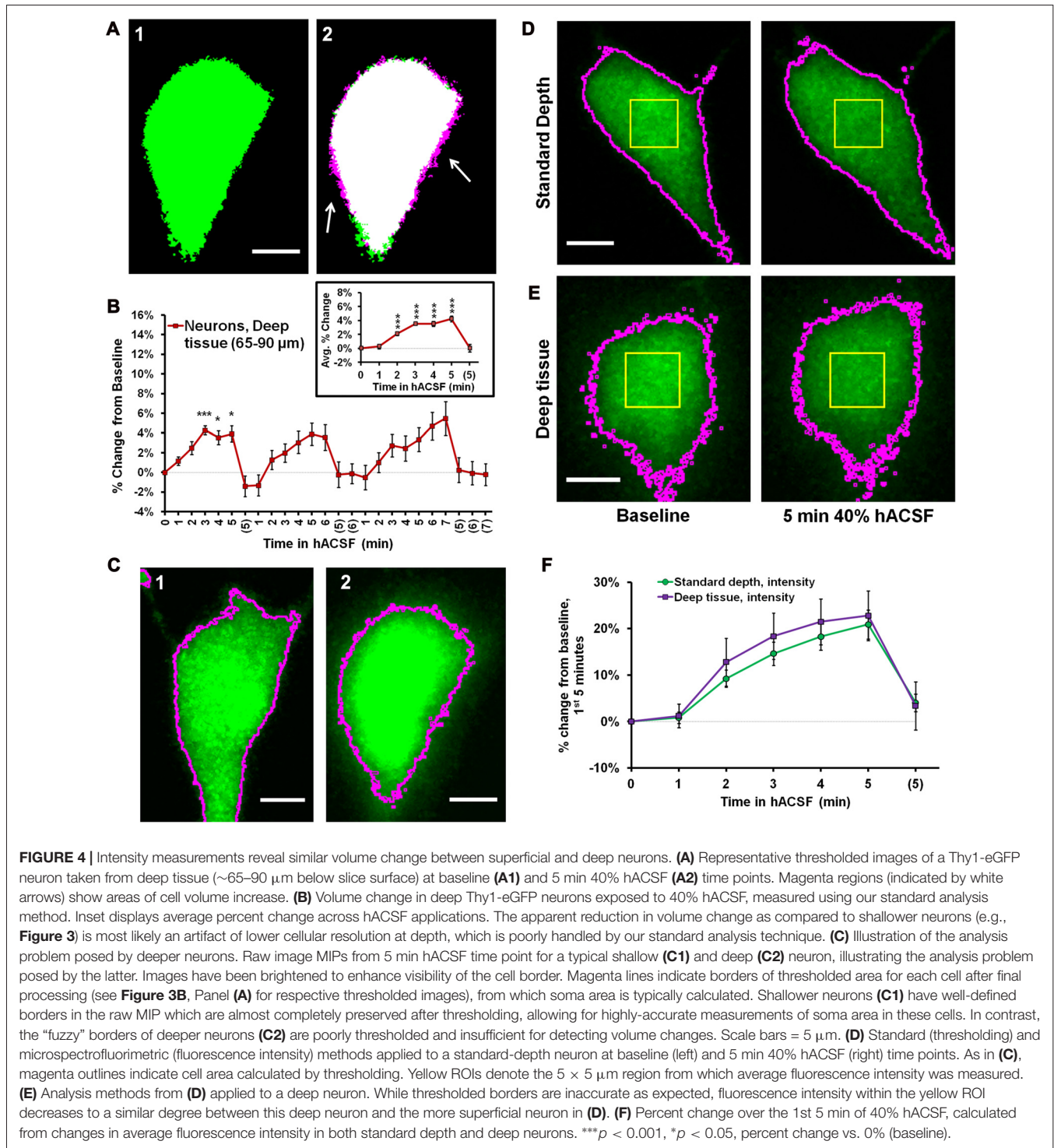


image did not fully represent the cell boundary (Figure 4C2). As the differences in cell volume are reflected in expansion

of the cell borders, such thresholding problems would likely result in underreporting of increases in cell volume and may explain the apparent reduction in volume change by deeper neurons.

In further support of this view, we observed that both shallow (Figure 4D) and deeper neurons (Figure 4E) consistently exhibited a visible, generally similar dimming of eGFP fluorescence during 40% hACSF application (compare average intensity change between (D) and (E)). This was a strong indicator that neurons at both depths were swelling to similar degrees, as demonstrated by the microspectrofluorimetric method of volume analysis used by Crowe et al. (1995). Broadly speaking, if intracellular dye content is constant (as can be assumed for eGFP molecules in a typical cell), then changes in intracellular water will alter dye concentration, which can be detected via changes in fluorescence intensity. Changes in fluorescence intensity ($\frac{F_t}{F_0}$, where F_0 is baseline fluorescence and F_t the fluorescence at a given time point) are inversely proportional to changes in cell volume (Crowe et al., 1995). We reasoned that this method should be much less sensitive to detection problems than our thresholding technique (magenta outlines, Figures 4D,E), since it would not be affected by the ability to resolve the cell boundary. To quantify the eGFP intensity shift, we used the pre-thresholding MIP time series for each cell (see “Materials and Methods” Section) to examine the intensity values of a $5 \times 5 \mu\text{m}$ region near the center of the cell (Yellow boxes, Figures 4D,E). Taking the reciprocal of the fluorescence ratio ($\frac{F_0}{F_t}$), we calculated a volume increase in deep neurons of over 20% by 5 min in 40% hACSF ($122.79 \pm 5.36\%$ of baseline, $n = 8$ cells; Figure 4F). Performing a similar measurement on neurons at our standard imaging depth (with the exception of two neurons in which eGFP was saturated and no F_0/F_t ratio could be obtained), we calculated a volume change nearly identical to that calculated in deep neurons ($120.90 \pm 3.14\%$ of baseline). It should be noted that although the F_0/F_t method of volume analysis has been previously used in slices (Risher et al., 2009), its accuracy in culture is much better established (Tuz et al., 2001; Benfenati et al., 2011), and the percentages calculated above should be considered only rough approximations of the true volume change. These data do, however, provide supportive evidence that *relative* volume changes in neurons exposed to 40% hACSF are independent of depth within the slice.

We also compared patch clamp-loaded astrocytes against those loaded with SR-101, a dye selectively taken up by astrocytes in the hippocampus (Schnell et al., 2012). SR-101-labeled astrocytes did not differ from patch-clamped astrocytes in their volume increase during 40% hACSF application (SR-101, $n = 10$; Patched, $n = 7$; $p = 0.401$; data not shown), although with repeated applications of hACSF they did appear to swell more than Thy1-eGFP neurons in the same conditions (in contrast with patch clamped astrocytes and neurons, which had shown no difference at either dose of hACSF). This effect was attributed largely to a slightly slower return to baseline in SR-101-labeled astrocytes, which caused a gradual “build



up” of astrocyte volume despite no change in average rate or degree of swelling. These tests overall provided clear evidence that neuronal swelling was not an artifact of neuronal damage due to whole-cell dialysis with fluorescent indicator, nor was it likely a result of the depth at which neurons resided in the tissue.

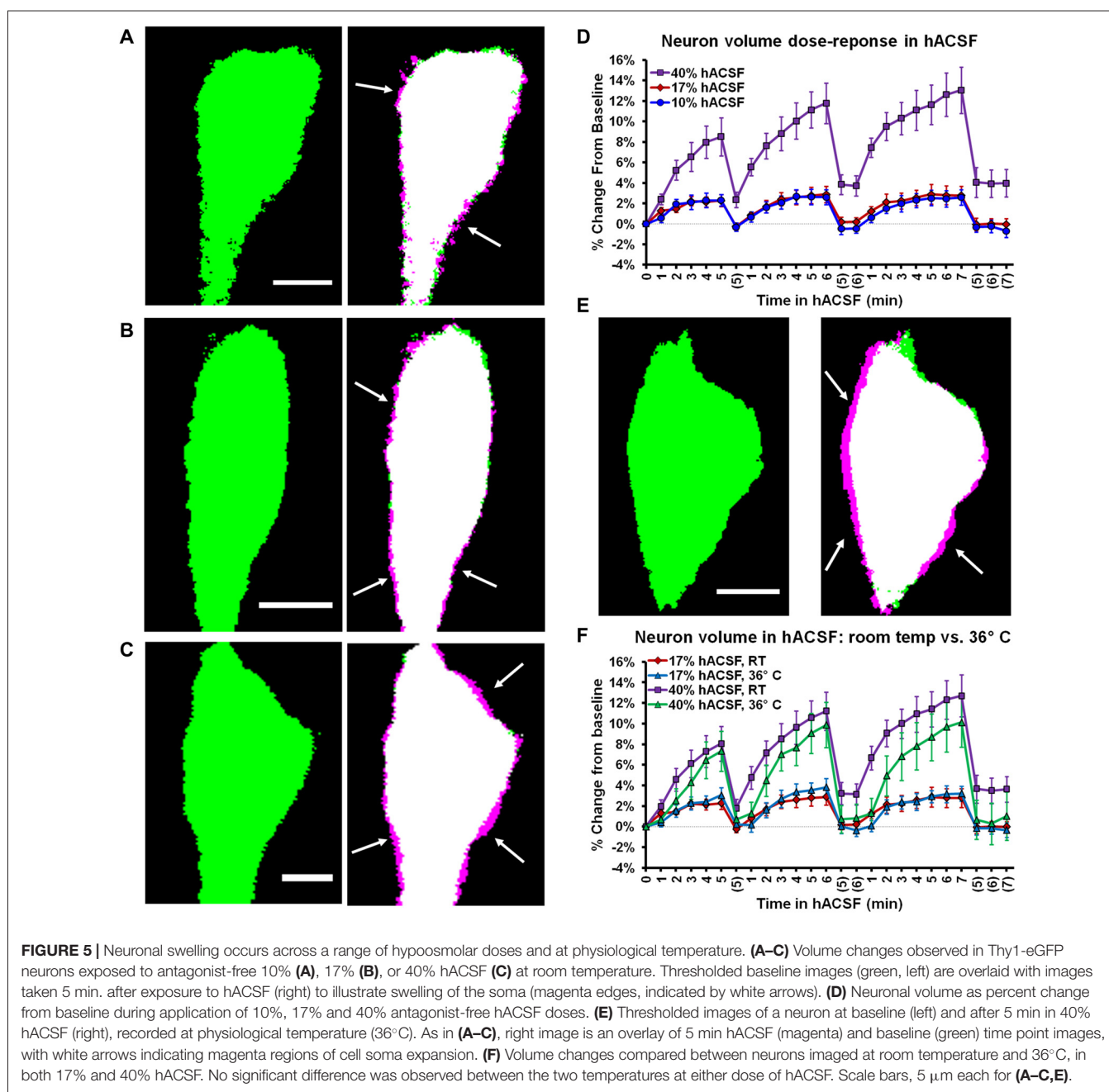
Neuronal Swelling Is Not due to Activation of AMPA Receptors or Action Potential-Mediated Synaptic Transmission

Having ruled out the possibility that neuronal swelling was an artifact of patch clamp, we next considered the specific composition of our solutions as a possible contributor. Until

this point, neuronal swelling had been observed in our standard hACSF, which contained 0 mM Mg^{2+} , 1 μ M TTX and 10 μ M NBQX. These conditions are ideal for isolating NMDA receptor-dependent SICs (Lauderdale et al., 2015), but are otherwise quite non-physiological. To determine if the composition of our hACSF was contributing to the observed neuronal swelling, we prepared “antagonist-free” hACSF solutions diluted directly from our standard ACSF (see “Materials and Methods” Section). Despite the removal of antagonists and partial restoration of Mg^{2+} , we continued to observe neuronal swelling across multiple doses of this more “physiological” hACSF (Figures 5A–C).

Neuronal swelling was partially dose-dependent (Figure 5D), differing significantly between 17% and 40% hACSF ($p = 0.005$), but not between 10% and 17% hACSF ($p = 0.935$). These results provide evidence that neuronal swelling is a direct result of reduced osmolarity rather than an artifact of any particular pharmacological reagent.

Cellular volume changes and volume regulation can be augmented by higher temperatures (Andrew et al., 1997, 1999). Therefore, neuronal volume changes might be negligible at physiological temperature due to more efficient volume regulatory mechanisms. To test this possibility, we performed



experiments at physiological temperature ($\sim 36^{\circ}\text{C}$). Neuronal swelling persisted in antagonist-free hACSF at physiological temperature (Figure 5E), and in fact there was no significant difference in neuronal swelling between 22°C and 36°C for either 17% hACSF ($F_{(1,13)} = 0.002$, $p = 0.967$) or 40% hACSF doses ($F_{(1,15)} = 1.521$, $p = 0.236$; Figure 5F). These results strongly argue against a contribution of temperature to the observed neuronal swelling.

Swelling Profiles of Layer V Cortical Pyramidal Neurons Differ from those of CA1 Pyramidal Neurons

Recent studies suggest considerable heterogeneity among neurons and astrocytes in different cortical regions, and previous work has indicated that cortical pyramidal neurons (Andrew et al., 2007), but not astrocytes (Risher et al., 2009) may be osmoresistant. To explore the possibility that swelling profiles of astrocytes and neurons are region-specific, we also measured volume changes in pyramidal neurons from neocortical layer V and passive astrocytes from layer II/III (Figure 6). We found eGFP expression to be particularly low in the cortex of Thy1-eGFP mice, which limited their utility for these experiments. Data were therefore pooled from Thy1-eGFP neurons ($n = 2$) and patch-clamped neurons ($n = 8$), and compared to pooled hippocampal neurons acquired using both techniques ($n = 9$ Thy1-eGFP, $n = 10$ patch clamp). As expected from our observations of hippocampal astrocytes and neurons, cortical layer II/III astrocytes (Figure 6A) and layer V pyramidal neurons (Figure 6B) both exhibited rapid volume changes upon exposure to antagonist-free 40% hACSF. Surprisingly, we observed significantly greater swelling in cortical neurons compared to cortical astrocytes (Figure 6C). Average percent change over three hACSF applications (Figure 6D) in cortical neurons was nearly double that of hippocampal neurons (5 min hACSF: CA1 neurons, $7.98 \pm 0.81\%$ increase; Cortical neurons, $14.18 \pm 0.98\%$ increase; $p < 0.001$). The average percent change did not differ between cortical vs. hippocampal astrocytes ($F_{(1,19)} = 0.43$, $p = 0.52$; Figure 6E). It was not immediately apparent whether the increase in cortical neuron osmosensitivity reflected an intrinsic difference in membrane properties, or simply a greater freedom for cell swelling due to the looser packing density of neurons in the cortex. These data suggest that osmosensitivity of pyramidal neurons varies by brain region, and importantly, that significant swelling of pyramidal neurons is not restricted to the hippocampal region.

Neuronal Swelling Is Not Due to NMDA Receptor Activation

In examining alternate explanations for neuronal swelling in hACSF, we next chose to more closely investigate the possible involvement of NMDA receptor excitotoxicity. Neuronal swelling is a well-established consequence of excitotoxic NMDA receptor activation (Rothman and Olney, 1987; Choi, 1992; Liang et al., 2007; Rungta et al., 2015), a distinct possibility in our conditions given the lack of Mg^{2+} in standard hACSF or 40% reduction of Mg^{2+} in physiological hACSF. Additionally,

we have previously established that large, NMDA receptor-dependent slow-inward currents (SICs) occur in hACSF (Fiacco et al., 2007; Lauderdale et al., 2015). While SIC frequency (Figure 7A) and amplitude (Figure 7B) can vary between multiple hACSF applications, their rapid appearance during hACSF (Figure 7C) correlates closely with the rapid time course of neuronal swelling and could indicate a common mechanism. To determine whether NMDA receptor activation contributes to neuronal swelling in 40% hACSF, we examined neuronal swelling in our standard hACSF conditions (0 mM Mg^{2+} , 1 μM TTX and 10 μM NBQX) with the addition of NMDA receptor inhibitors. Despite the similar circumstances under which SICs and neuronal swelling are observed, we found that neither the selective NMDA receptor antagonist DL-2-Amino-5-phosphonopentanoic acid (DL-AP5; 50 μM), nor 6 mM Mg^{2+} , both of which entirely block NMDA receptor-dependent currents (Dissing-Olesen et al., 2014; Lauderdale et al., 2015), had any effect on neuronal swelling in 40% hACSF ($F_{(2,20)} = 0.06$, $p = 0.942$; Figure 7D). These data suggest that neuronal swelling occurs independently of NMDA receptor activation.

Neuronal and Glial Swelling Occur in Tissue from Both Juvenile and Adult Mice

We next considered the possibility that neuronal osmosensitivity varied as a function of age. All of our experiments to this point had been performed in slices from P15 to P21 juvenile mice. To test the possibility that neuronal swelling was an age-dependent effect, we repeated experiments using adult (10–15 week old) mice (Figure 8). Once again antagonist-free 40% hACSF was prepared, as the inclusion of Mg^{2+} and lack of antagonists provided greater physiological relevance for our results while enabling direct comparison to results from previous studies (Andrew et al., 2007; Risher et al., 2009). As we had observed in juveniles, both adult CA1 neurons and s.r. astrocytes swelled rapidly in response to 40% hACSF application (Figure 8A), and did not differ significantly in their time courses ($F_{(1,17)} = 0.61$, $p = 0.447$). Comparison of average percent change between adults and juveniles (Figures 8B,C) revealed no significant differences in neuronal swelling ($F_{(1,16)} = 0.09$, $p = 0.773$) or astrocyte swelling ($F_{(1,19)} = 0.006$, $p = 0.94$) between the two age groups. These findings suggest that neuronal swelling is not a developmental phenomenon.

Hypoosmolar Swelling of Neurons and Astrocytes Does Not Require AQP4

In astrocytes, water permeability is thought to be regulated by the expression and gating of AQP4 channels (Nagelhus et al., 2004; Gunnarson et al., 2008; Song and Gunnarson, 2012). Functional water channels have not been found in pyramidal neurons, a proposed reason behind their apparent resistance to osmotic stress (Gorelick et al., 2006; Andrew et al., 2007). Our observation of neuronal swelling in all hACSF conditions, however, was clear evidence that the lack of functional aquaporins was not a limiting factor for cell volume change in neurons, and that water must be entering through an alternate route. Several of the alternate, AQP4-independent mechanisms proposed for swelling

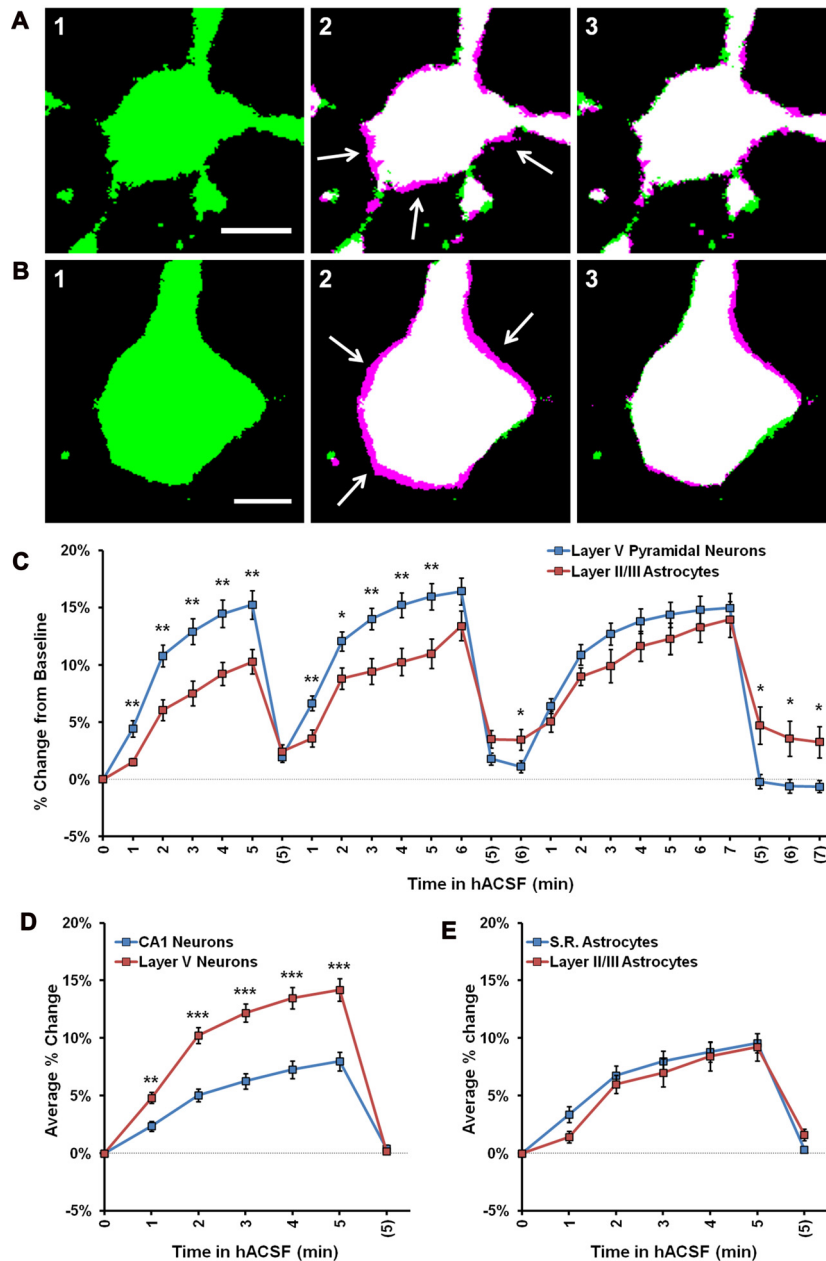
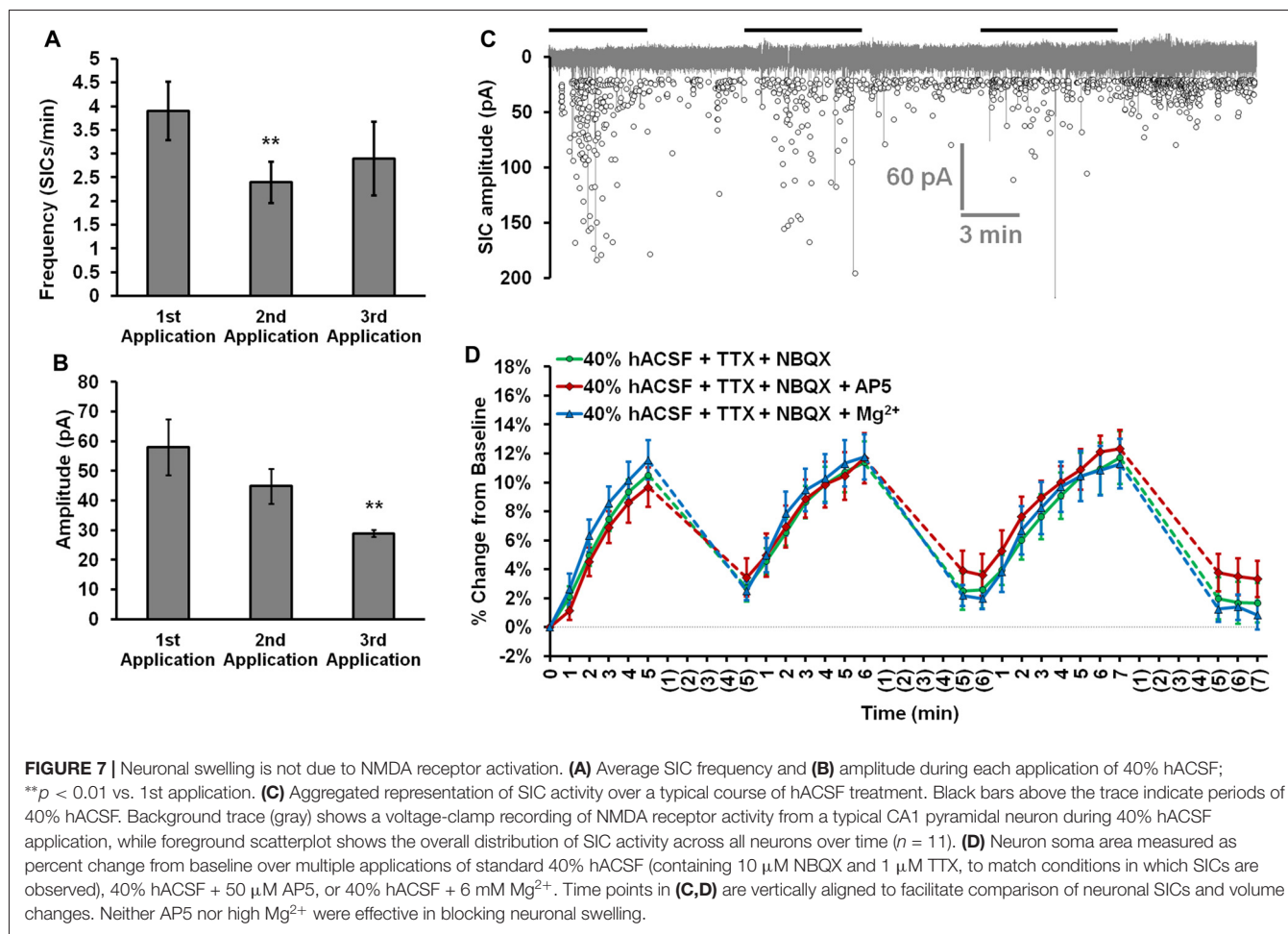


FIGURE 6 | Cortical neurons swell significantly more than cortical astrocytes in 40% hACSF. **(A)** Representative thresholded image of an astrocyte from cortical layer II/III at baseline **(A1)**, overlaid with an image after 5 min in antagonist-free 40% hACSF **(A2)** and after 5 min of return to standard ACSF **(A3)**. **(B)** Representative pyramidal neuron from cortical layer V at baseline **(B1)**, overlaid with 5 min antagonist-free 40% hACSF **(B2)** and 5 min standard ACSF wash **(B3)** time point images, as in **(A)**. Magenta highlights surrounding the cell border in **(A2)** and **(B2)**, indicated by white arrows, reflect increases in cell volume over baseline. Scale bars, 5 μ m. **(C)** Percent change from baseline quantified for cortical (Layer V) neurons and cortical (layer II/III) astrocytes. Note that cortical neurons swell significantly more than astrocytes during the first two applications of hACSF. **(D)** Comparisons of average percent change over the three hACSF applications reveal that cortical neurons swell to approximately twice the size of hippocampal neurons in hACSF, while cortical astrocytes **(E)** show similar responses as hippocampal astrocytes. * $p < 0.05$, ** $p < 0.01$, *** $p < 0.001$, layer V neurons vs.: layer II/III astrocytes **(C)** or CA1 neurons **(D)**.

in astrocytes, including water-permeable cotransporters and even water flux directly across the cell membrane (Kimelberg, 2005), could also be functional in neurons and contribute to the observed neuronal swelling in our conditions. If these

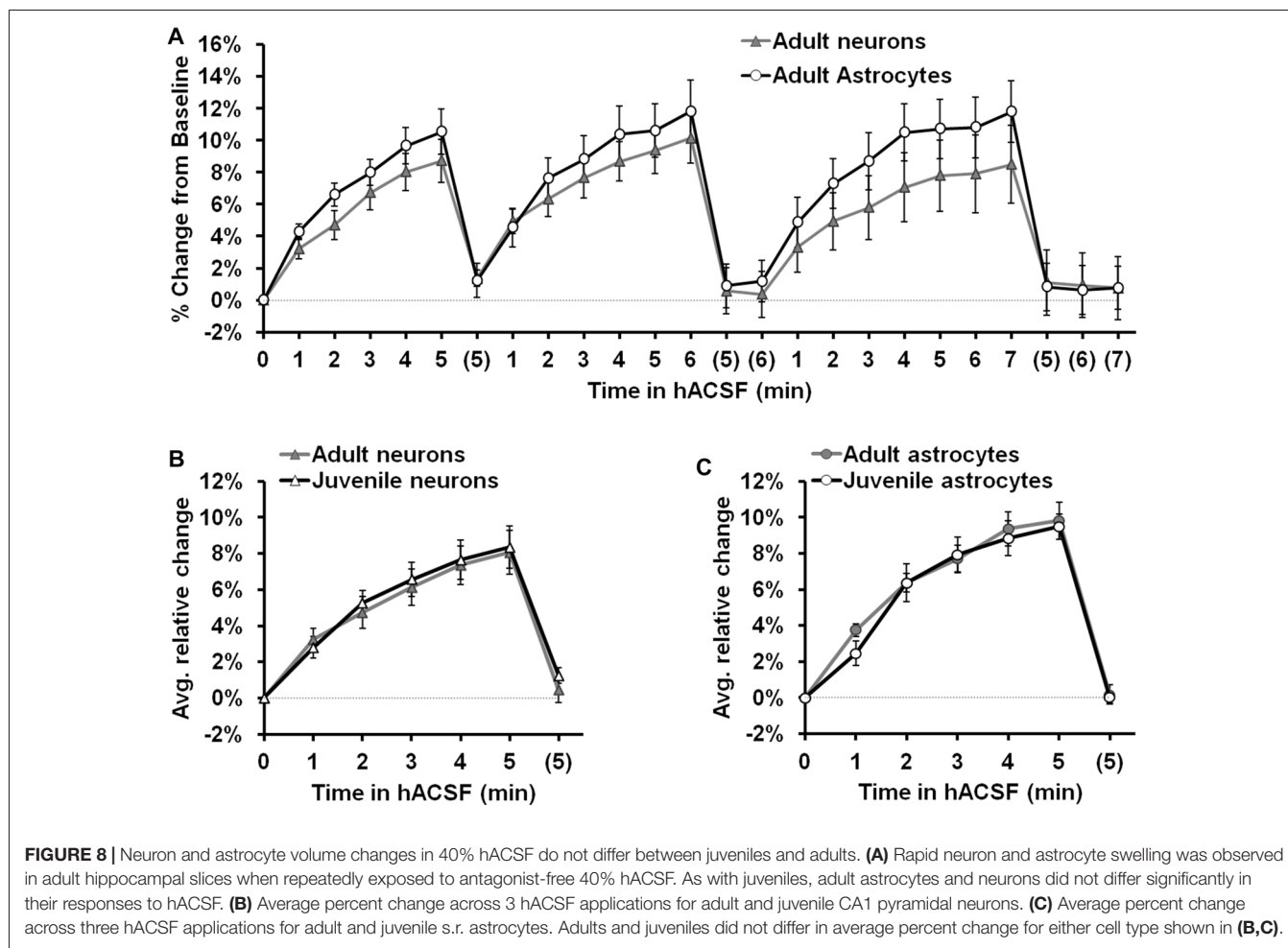
AQP4-independent mechanisms mediate the rapid neuronal swelling in our hACSF, it follows that the rapid astrocyte swelling in our hACSF may also be partially (or fully) independent of AQP4.



We therefore examined the acute volume responses of both CA1 pyramidal neurons and s.r. astrocytes to antagonist-free hACSF, using hippocampal slices from $AQP4^{-/-}$ mice (Figure 9). As foreshadowed by our neuronal data gathered to this point, astrocytes continued to swell even in the absence of AQP4, implying rapid astrocyte volume changes occur independently of AQP4 expression (Figure 9A). Surprisingly however, $AQP4^{-/-}$ astrocytes swelled significantly more in 40% hACSF compared to wild-type, reaching approximately 1.4 times the volume of wild-type astrocytes by the end of each hACSF application (Figure 9B; $AQP4^{-/-}$, $113.19\% \pm 0.92\%$; WT, $109.71\% \pm 0.54\%$; $p = 0.005$). By contrast, astrocyte swelling did not differ between $AQP4^{-/-}$ and wild-type astrocytes in 17% hACSF ($F_{(1,17)} = 1.000$, $p = 0.331$). We also tested the effects of $AQP4^{-/-}$ on neuronal volume changes in 40% hACSF. Not surprisingly, AQP4 deletion had no effect on neuronal swelling ($F_{(1,16)} = 0.02$, $p = 0.891$; Figures 9C,D). These data seemed to indicate that AQP4 expression, far from being *required* for intracellular accumulation of water in astrocytes, may actually play an important role in *limiting* the degree of swelling during severe hypoosmolar stress. Overall, our results strongly suggest that water influx resulting from hACSF application is not selective to astrocytes, and is not mediated by AQP4.

DISCUSSION

The major finding in this study is that CA1 pyramidal neurons readily swell in hypoosmolar conditions, increasing their volume significantly above baseline even within the first minute of hACSF application. The rate and overall amount of neuronal swelling was found to be almost identical to that observed in stratum radiatum astrocytes, and was observed repeatedly across a variety of experimental conditions. Neuronal swelling was rapidly reversible, returning to baseline after 5–7 min in normosmolar ACSF, and readily returned upon re-application of hACSF. While the astrocyte swelling observed is in line with the reportedly high osmosensitivity of astrocytes and astrocyte-like glial cells (Hirrlinger et al., 2008; Risher et al., 2009), the neuronal swelling observed contrasts with previous work concluding that neurons steadfastly retain their volume during osmotic challenge (Andrew et al., 2007; Caspi et al., 2009). Neither glial nor neuronal swelling was found to require AQP4 expression. These data cast doubt over the commonly-accepted roles of neurons and astrocytes in brain water regulation. Cellular volume increases following acute reductions in extracellular osmolarity may be a fundamental property of both pyramidal neurons and astrocytes, an



important consideration in brain pathologies involving cellular edema.

The possibility that neuronal volume changes are extremely sensitive to subtle differences in methodology was strongly considered and systematically examined in this study. Initial experiments were performed in tissue slices from juvenile mice at room temperature, using whole-cell patch clamp to dialyze individual CA1 hippocampal cells located 30–50 μm from the slice surface with fluorescent dye. These conditions differed substantially from those of Andrew et al. (2007), the study most widely cited as concrete evidence of neuronal osmoresistance. For example, Andrew et al. (1997) performed experiments at 33–34°C based on a previous observation that slice swelling is noticeably decreased at higher temperatures, a possible indicator of isovolumetric regulation (IVR) which is characterized by an apparent resistance to volume change (Lohr and Grantham, 1986; Franco et al., 2000; Tuz et al., 2001; Pasantes-Morales and Tuz, 2006). Furthermore, IVR is observed only during gradual (but not sudden) shifts in osmolarity (Franco et al., 2000; Tuz et al., 2001; Pasantes-Morales and Tuz, 2006). Neurons imaged deeper in tissue would likely be exposed to more gradual solution exchanges and therefore, more gradual changes in osmolarity which could reduce the rate of swelling and facilitate

IVR. Therefore, to specifically test the role of these and other variables, additional recordings were performed in the following conditions: (1) using Thy 1-eGFP transgenic mice (Feng et al., 2000; Andrew et al., 2007) to avoid possible cell damage from patch clamp; (2) at physiological temperature (36°C); (3) in deep tissue (65–90 μm); (4) in slices from adult (10–15 week old) mice; and (5) in the neocortex. Neuronal swelling was observed across all of these conditions, suggesting that it may be a ubiquitous response to reductions in osmolarity in both juvenile and adult tissue.

Using our standard volume analysis protocol, we found that swelling of neurons located deeper in the tissue (65–90 μm) was more difficult to observe compared to superficial neurons. We interpret much of this apparent difference as a loss of image fidelity rather than a true effect of tissue depth on volume changes. This interpretation is supported by our observation that changes in cell fluorescence intensity over time (which are inversely related to changes in cell volume; Crowe et al., 1995) did not significantly differ between superficial and deep neurons—a strong indication that neurons at both depths were swelling to similar volumes.

It is worth noting that our standard image analysis protocol, although based on established methods (Hirrlinger et al., 2008;

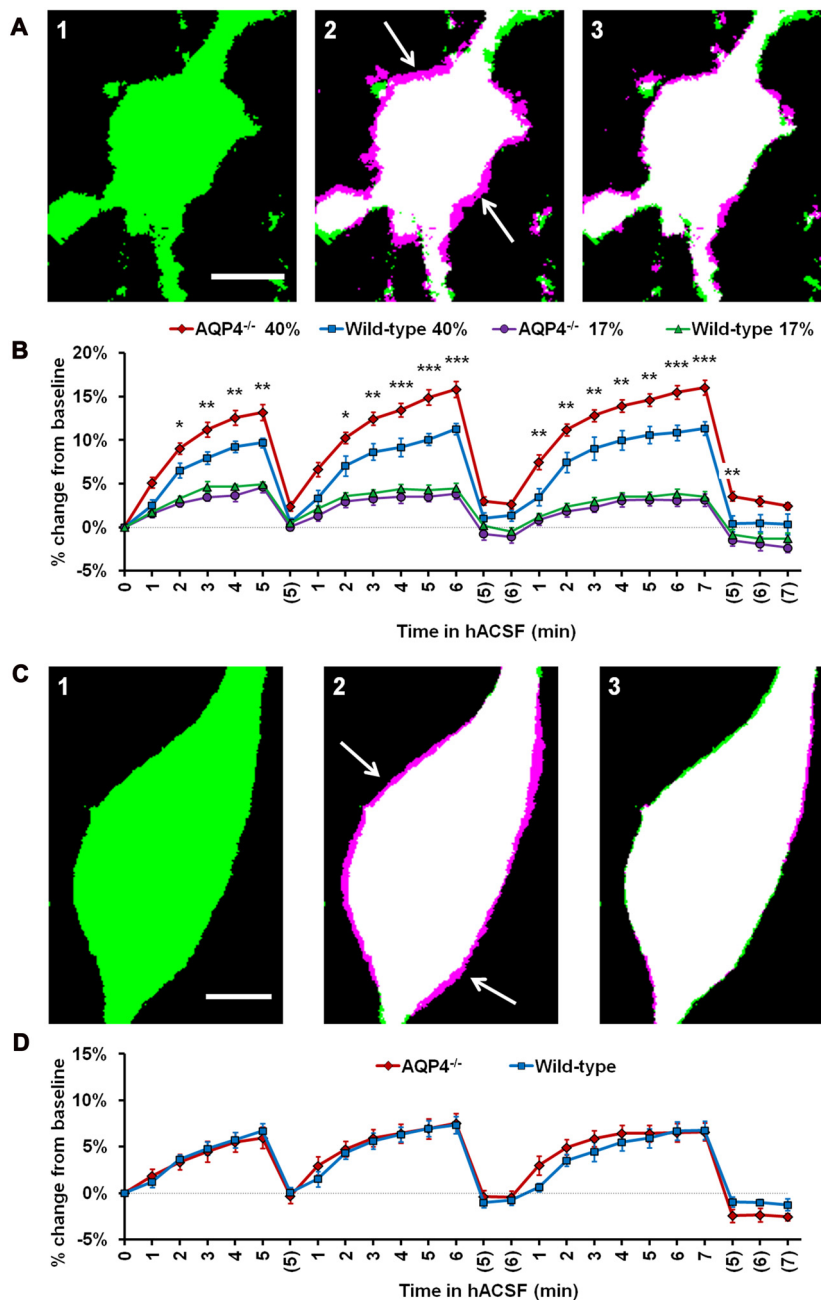


FIGURE 9 | Astrocyte volume changes do not require expression of aquaporin-4 (AQP4). **(A)** Representative thresholded images of an AQP4^{-/-} astrocyte soma at baseline **(A1)**, overlaid with an image after 5 min in antagonist-free 40% hACSf **(A2)** and after 5 min wash in standard ACSf **(A3)**. As in previous figures, magenta regions (indicated by white arrows) represent increases in volume over baseline. **(B)** Astrocyte volume, quantified as percent change from baseline, in AQP4^{-/-} and wild-type astrocytes exposed to 17% or 40% hACSf. AQP4^{-/-} astrocytes showed no change in swelling at 17% hACSf and significantly greater swelling at 40% hACSf, as compared to wild-type. **(C)** Representative thresholded images and overlays of an AQP4^{-/-} neuron soma at baseline **(C1)**, after 5 min in antagonist-free 40% hACSf **(C2)**, and after a 5 min wash period in standard ACSf **(C3)**. **(D)** Volume changes in hACSf are compared between AQP4^{-/-} and wild-type neurons. As expected, neuronal swelling did not differ significantly between these two genotypes. **p* < 0.05, ***p* < 0.01, and ****p* < 0.001 vs. wild-type astrocytes in 40% hACSf. Scale bars, 5 μm each for **(A,C)**.

Risher et al., 2009, 2012), was intentionally conservative and likely underestimates actual changes in cell volume. Cell soma area was chosen as a proxy for overall volume changes, since

direct measures of cell volume were not feasible for our conditions. Assuming that cell volume is changing equally in all directions, it can be inferred that our measurements reflect

only about two-thirds of the true change in volume. This inference is partially supported by the analysis of fluorescence intensity as an indication of cell volume changes, which suggested volume increases >1.5 times those calculated from thresholded images. We also observed that the precise method of image processing had a surprisingly strong impact on measured volume. The overall magnitude of volume change observed could often be increased twofold or more simply through the use of different thresholding methods. These apparent increases in signal-to-noise ratio often came at the expense of “cell” and “background” pixels being incorrectly classified, and the thresholded images inconsistent with what could be observed “by eye” pre-thresholding (unpublished observations). We therefore rejected these methods in favor of the more conservative “mean” thresholding method, which more consistently returned an image in which the cell body could be clearly identified.

One of the more exciting findings in the present study was a lack of evidence for AQP4-mediated water *influx* into astrocytes or neurons exposed to hACSF. While not necessarily surprising for neurons, which do not express AQP4 (Nielsen et al., 1997), lack of inhibition of astrocyte swelling in AQP4^{-/-} mouse tissue was rather unexpected based on a large body of literature on the requirement of AQP4 for facilitated water movement across the astrocyte membrane. Surprisingly, not only was AQP4 not required for astrocyte swelling, but astrocyte volume in severely (40%) hypoosmolar conditions was significantly greater in AQP4^{-/-} mice compared to wild-type animals. There are a couple of potential explanations for this finding.

First, AQP4^{-/-} animals have been shown to have a nearly 30% larger resting brain ECS compared to wild-type animals (Binder et al., 2004; Yao et al., 2008). It is possible that the enlarged ECS in AQP4^{-/-} mice provides more available space for astrocytes to swell into, leading to increased astrocyte swelling. This explanation, however, fails to account for the lack of increased neuronal swelling in AQP4^{-/-} mice, since neurons would presumably also be adjacent to increased ECS. It is also unlikely that astrocyte volume changes in our 40% hACSF were limited by the ECS in wild-type animals, as tissue continues to swell in far more severe hypoosmolar conditions (Chebabo et al., 1995b).

A second explanation is that AQP4 can provide an efficient efflux pathway for water to leave astrocytes. AQP4 expression is polarized, with highest levels of expression in perivascular endfeet (Nielsen et al., 1997). Loss of AQP4 at endfeet has been proposed to inhibit water removal from the astrocyte, leading to increased swelling (Wetherington et al., 2008) and impairing tissue recovery from vasogenic edema (Papadopoulos et al., 2004). Recent work demonstrates AQP4-dependent water efflux may also be important physiologically. Haj-Yasein et al. (2012, 2015) observed that Schaffer collateral stimulation in AQP4^{-/-} hippocampal slices resulted in a greater ECS reduction (indicating increased cell swelling), and higher peak $[K^+]_o$ compared to slices from wild-type mice. The authors concluded that ECS shrinkage (caused by activity-dependent astrocyte water uptake) is normally offset by an osmotically-driven water efflux through perisynaptic AQP4 channels.

Our findings suggest that bath application of hACSF into the slice similarly produces a rapid AQP4-independent influx of water into the astrocyte, from which it cannot efficiently escape because the AQP4 efflux pathway has been removed.

Interestingly, some recent studies suggest that rapid water influx through AQP4 may be important for opening stretch activated channels which facilitate intracellular osmolyte efflux and volume regulation of astrocytes (Benfenati et al., 2011; Jo et al., 2015; Mola et al., 2016). IVR, which is associated with osmolyte efflux into the ECS and is known to occur in glial cells, may be partially dependent on such a mechanism (Franco et al., 2000; Lohr and Yohe, 2000). IVR is easily overwhelmed by more rapid or larger osmotic shifts (Lohr and Yohe, 2000), which may explain the lack of visible IVR in the current study. Thus, it is possible that volume regulatory mechanisms are actively resisting volume change in wild-type astrocytes, and that such mechanisms are impaired in AQP4^{-/-} astrocytes. Regardless of underlying mechanism, our findings suggest that: (a) AQP4 is not required for rapid water influx into CA1 neurons or astrocytes; and (b) AQP4 may serve as an important water *efflux* pathway that helps limit the extent of astrocyte swelling.

The observation that the effects of AQP4^{-/-} on astrocyte swelling are hACSF dose-dependent is not unprecedented. Thrane et al. (2011) observed a reduction in AQP4^{-/-} astrocyte swelling in 20% hACSF, but no difference in 30% hACSF. A direct comparison of their findings to ours is somewhat complicated, as Thrane et al. (2011) used different hACSF doses and longer imaging intervals (5–10 min) relative to ours. Based on the direction of the effect of AQP4 deletion on astrocyte swelling, however, it is tempting to speculate that Thrane et al. (2011) might have also observed augmented astrocyte swelling in 40% hACSF. It is also important to note that Thrane et al. (2011) measured AQP4^{-/-} astrocyte volume in the cortex, while we recorded effects on s.r. astrocytes in CA1. AQP4 expression levels and patterns are quite distinct between these two regions (Hubbard et al., 2015), and it is possible that the role of AQP4 in water movement is also brain region-dependent. Although the exact effects of AQP4 deletion on astrocyte swelling differed between the two sets of data, both suggest that the role of AQP4 in water movement is governed by the severity of the osmotic challenge.

If neurons are indeed swelling in hACSF, then what is the route of water influx? Clues to this answer may lie in other conditions which cause neuronal swelling. While hypoosmolar swelling has generally been reported only in dissociated neurons *in vitro* (Aitken et al., 1998; Somjen, 1999; Inoue et al., 2005; Boss et al., 2013), pyramidal neurons have long been known to swell in excitotoxic conditions (Choi, 1992; Risher et al., 2009; Zhou et al., 2010). Massive intracellular sodium influx (as observed in cases of continuous neuronal firing or excessive NMDA receptor activation) can cause sufficient depolarization to open voltage-gated Cl⁻ channels, with the resulting increase in intracellular osmolarity (from both Na⁺ and Cl⁻) producing an osmotic gradient into the neuron (Rungta et al., 2015). This highlights

the fact that, despite lacking functional water channels, neurons are capable of taking on water through alternate means quite rapidly. Consistent with this, spreading depression (a wave of depolarization, excessively high K^+ and glutamate release in the ECS) has been reported in hypoosmolar conditions (Chebabo et al., 1995a; Huang et al., 1995) and can induce excitotoxic neuronal swelling (Zhou et al., 2010). There is little reason to believe an excitotoxic mechanism is directly responsible for the observed neuronal swelling in our model, as it was unaffected by NMDA receptor blockers, and we have previously found no evidence of spreading depression in hACSF (Lauderdale et al., 2015). Instead, we propose that the osmotic gradient, which drives water into a neuron following excessive Na^+ and Cl^- influx (Rungta et al., 2015), parallels the gradient imposed by hACSF on a neuron with normal intracellular ion concentrations. Routes for such water influx into neurons are not well defined. Two possible routes might be inferred from the known or hypothesized AQP4-independent pathways for water influx into astrocytes: simple water diffusion across the plasma membrane (Kimelberg, 2005; Papadopoulos and Verkman, 2013), or water movement through a commonly-expressed cotransporter such as the Na^+ , K^+ , $2Cl^-$ cotransporter NKCC1 (MacVicar et al., 2002; Su et al., 2002a,b; Yan et al., 2003; Kimelberg, 2005; Jayakumar and Norenberg, 2010; MacAulay and Zeuthen, 2012). Neither of these water pathways is likely to be exclusive to astrocytes, and the similarity in swelling profiles between pyramidal neurons and astrocytes in our standard hACSF

conditions might suggest a common mechanism independent of AQP4. Future studies will explore potential mechanisms of water influx into astrocytes and neurons in hypoosmolar conditions.

AUTHOR CONTRIBUTIONS

TAF conceived of and guided the project. TAF and TRM designed and developed experiments and wrote the manuscript. DD, NC, LRY and DKB provided feedback on experiments and manuscript. AQP4-null mice were provided by DKB. TRM, DD and NC acquired imaging data. TRM developed image analysis protocols and ran statistics. TRM, DD, NC and LRY analyzed imaging data. KL acquired and analyzed electrophysiology data, and provided helpful feedback on statistics.

FUNDING

This work was supported by the National Institutes of Health National Institute of Neurological Disorders and Stroke (NINDS) R01NS082570.

SUPPLEMENTARY MATERIAL

The Supplementary Material for this article can be found online at: <http://journal.frontiersin.org/article/10.3389/fncel.2017.00275/full#supplementary-material>

REFERENCES

- Aitken, P. G., Borgdorff, A. J., Jutta, A. J., Kiehart, D. P., Somjen, G. G., and Wadman, W. J. (1998). Volume changes induced by osmotic stress in freshly isolated rat hippocampal neurons. *Pflügers Arch.* 436, 991–998. doi: 10.1007/s004240050734
- Amiry-Moghaddam, M., Williamson, A., Palomba, M., Eid, T., de Lanerolle, N. C., Nagelhus, E. A., et al. (2003). Delayed K^+ clearance associated with aquaporin-4 mislocalization: phenotypic defects in brains of α -syn-trophin-null mice. *Proc. Natl. Acad. Sci. U S A* 100, 13615–13620. doi: 10.1073/pnas.2336064100
- Anderova, M., Benesova, J., Mikesova, M., Dzamba, D., Honsa, P., Kriska, J., et al. (2014). Altered astrocytic swelling in the cortex of α -syn-trophin-negative GFAP/EGFP mice. *PLoS One* 9:e113444. doi: 10.1371/journal.pone.0119744
- Andrew, R. D. (1991). Seizure and acute osmotic change: clinical and neurophysiological aspects. *J. Neurol. Sci.* 101, 7–18. doi: 10.1016/0022-510x(91)90013-w
- Andrew, R. D., Jarvis, C. R., and Obeidat, A. S. (1999). Potential sources of intrinsic optical signals imaged in live brain slices. *Methods* 18, 185–196. doi: 10.1006/meth.1999.0771
- Andrew, R. D., Labron, M. W., Boehnke, S. E., Carnduff, L., and Kirov, S. A. (2007). Physiological evidence that pyramidal neurons lack functional water channels. *Cereb. Cortex* 17, 787–802. doi: 10.1093/cercor/bhk032
- Andrew, R. D., Lobinowich, M. E., and Osehobo, E. P. (1997). Evidence against volume regulation by cortical brain cells during acute osmotic stress. *Exp. Neurol.* 143, 300–312. doi: 10.1006/exnr.1996.6375
- Andrew, R. D., and MacVicar, B. A. (1994). Imaging cell volume changes and neuronal excitation in the hippocampal slice. *Neuroscience* 62, 371–383. doi: 10.1016/0306-4522(94)90372-7
- Azouz, R., Alroy, G., and Yaari, Y. (1997). Modulation of endogenous firing patterns by osmolarity in rat hippocampal neurons. *J. Physiol. Lond.* 502, 175–187. doi: 10.1111/j.1469-7793.1997.175bl.x
- Benfenati, V., Caprini, M., Dovizio, M., Mylonakou, M. N., Ferroni, S., Ottersen, O. P., et al. (2011). An aquaporin-4/transient receptor potential vanilloid 4 (AQP4/TRPV4) complex is essential for cell-volume control in astrocytes. *Proc. Natl. Acad. Sci. U S A* 108, 2563–2568. doi: 10.1073/pnas.1012867108
- Binder, D. K., Papadopoulos, M. C., Haggie, P. M., and Verkman, A. S. (2004). *In vivo* measurement of brain extracellular space diffusion by cortical surface photobleaching. *J. Neurosci.* 24, 8049–8056. doi: 10.1523/jneurosci.2294-04.2004
- Borgdorff, A. J., Somjen, G. G., and Wadman, W. J. (2000). Two mechanisms that raise free intracellular calcium in rat hippocampal neurons during hypoosmotic and low NaCl treatment. *J. Neurophysiol.* 83, 81–89.
- Boss, D., Kühn, J., Jourdain, P., Depeursinge, C., Magistretti, P. J., and Marquet, P. (2013). Measurement of absolute cell volume, osmotic membrane water permeability, and refractive index of transmembrane water and solute flux by digital holographic microscopy. *J. Biomed. Opt.* 18:036007. doi: 10.1117/1.jbo.18.3.036007
- Caspi, A., Benninger, F., and Yaari, Y. (2009). $Kv7/M$ channels mediate osmotic modulation of intrinsic neuronal excitability. *J. Neurosci.* 29, 11098–11111. doi: 10.1523/jneurosci.0942-09.2009
- Castilla-Guerra, L., del Carmen Fernández-Moreno, M., López-Chozas, J. M., and Fernández-Bolaños, R. (2006). Electrolytes disturbances and seizures. *Epilepsia* 47, 1990–1998. doi: 10.1111/j.1528-1167.2006.00861.x
- Chebabo, S. R., Hester, M. A., Aitken, P. G., and Somjen, G. G. (1995a). Hypotonic exposure enhances synaptic transmission and triggers spreading depression in rat hippocampal tissue slices. *Brain Res.* 695, 203–216. doi: 10.1016/0006-8993(95)00778-0
- Chebabo, S. R., Hester, M. A., Jing, J., Aitken, P. G., and Somjen, G. G. (1995b). Interstitial space, electrical resistance and ion concentrations during hypotonia of rat hippocampal slices. *J. Physiol.* 487, 685–697. doi: 10.1113/jphysiol.1995.sp020910
- Choi, D. W. (1992). Excitotoxic cell death. *J. Neurobiol.* 23, 1261–1276. doi: 10.1002/neu.480230915

- Crowe, W. E., Altamirano, J., Huerto, L., and Alvarez-Leefmans, F. J. (1995). Volume changes in single N1E-115 neuroblastoma cells measured with a fluorescent probe. *Neuroscience* 69, 283–296. doi: 10.1016/0306-4522(95)00219-9
- Darby, M., Kuzmiski, J. B., Panenka, W., Feighan, D., and MacVicar, B. A. (2003). ATP released from astrocytes during swelling activates chloride channels. *J. Neurophysiol.* 89, 1870–1877. doi: 10.1152/jn.00510.2002
- Dissing-Olesen, L., LeDue, J. M., Rungta, R. L., Hefendehl, J. K., Choi, H. B., and MacVicar, B. A. (2014). Activation of neuronal NMDA receptors triggers transient ATP-mediated microglial process outgrowth. *J. Neurosci.* 34, 10511–10527. doi: 10.1523/jneurosci.0405-14.2014
- Eid, T., Lee, T. S., Thomas, M. J., Amiry-Moghaddam, M., Bjornsen, L. P., Spencer, D. D., et al. (2005). Loss of perivascular aquaporin 4 may underlie deficient water and K⁺ homeostasis in the human epileptogenic hippocampus. *Proc. Natl. Acad. Sci. U S A* 102, 1193–1198. doi: 10.1073/pnas.0409308102
- Feng, G., Mellor, R. H., Bernstein, M., Keller-Peck, C., Nguyen, Q. T., Wallace, M., et al. (2000). Imaging neuronal subsets in transgenic mice expressing multiple spectral variants of GFP. *Neuron* 28, 41–51. doi: 10.1016/s0896-6273(00)00084-2
- Fiacco, T. A., Agulhon, C., Taves, S. R., Petravicz, J., Casper, K. B., Dong, X., et al. (2007). Selective stimulation of astrocyte calcium *in situ* does not affect neuronal excitatory synaptic activity. *Neuron* 54, 611–626. doi: 10.1016/j.neuron.2007.04.032
- Franco, R., Quesada, O., and Pasantes-Morales, H. (2000). Efflux of osmolyte amino acids during isovolumic regulation in hippocampal slices. *J. Neurosci. Res.* 61, 701–711. doi: 10.1002/1097-4547(20000915)61:6<701::aid-jnr14>3.3.co;2-k
- Gorelick, D. A., Praetorius, J., Tsunenari, T., Nielsen, S., and Agre, P. (2006). Aquaporin-11: a channel protein lacking apparent transport function expressed in brain. *BMC Biochem.* 7:14. doi: 10.1186/1471-2091-7-14
- Gunnarson, E., Zelenina, M., Axehult, G., Song, Y., Bondar, A., Krieger, P., et al. (2008). Identification of a molecular target for glutamate regulation of astrocyte water permeability. *Glia* 56, 587–596. doi: 10.1002/glia.20627
- Hagos, L., and Hülsmann, S. (2016). Unspecific labelling of oligodendrocytes by sulforhodamine 101 depends on astrocytic uptake via the thyroid hormone transporter OATP1C1 (SLC01C1). *Neurosci. Lett.* 631, 13–18. doi: 10.1016/j.neulet.2016.08.010
- Haj-Yasein, N. N., Bugge, C. E., Jensen, V., Østby, I., Ottersen, O. P., Hvalby, Ø., et al. (2015). Deletion of aquaporin-4 increases extracellular K⁺ concentration during synaptic stimulation in mouse hippocampus. *Brain Struct. Funct.* 220, 2469–2474. doi: 10.1007/s00429-014-0767-z
- Haj-Yasein, N. N., Jensen, V., Østby, I., Omholt, S. W., Voipio, J., Kaila, K., et al. (2012). Aquaporin-4 regulates extracellular space volume dynamics during high-frequency synaptic stimulation: a gene deletion study in mouse hippocampus. *Glia* 60, 867–874. doi: 10.1002/glia.22319
- Haskew-Layton, R. E., Rudkouskaya, A., Jin, Y., Feustel, P. J., Kimelberg, H. K., and Mongin, A. A. (2008). Two distinct modes of hypoosmotic medium-induced release of excitatory amino acids and taurine in the rat brain *in vivo*. *PLoS One* 3:e3543. doi: 10.1371/journal.pone.0003543
- Hill, R. A., and Grutzendler, J. (2014). *In vivo* imaging of oligodendrocytes with sulforhodamine 101. *Nat. Methods* 11, 1081–1082. doi: 10.1038/nmeth.3140
- Hirrlinger, P. G., Wurm, A., Hirrlinger, J., Bringmann, A., and Reichenbach, A. (2008). Osmotic swelling characteristics of glial cells in the murine hippocampus, cerebellum, and retina *in situ*. *J. Neurochem.* 105, 1405–1417. doi: 10.1111/j.1471-4159.2008.05243.x
- Huang, R., Aitken, P. G., and Somjen, G. G. (1995). The extent and mechanism of the loss of function caused by strongly hypotonic solutions in rat hippocampal slices. *Brain Res.* 695, 195–202. doi: 10.1016/0006-8993(95)00777-n
- Hubbard, J. A., Hsu, M. S., Seldin, M. M., and Binder, D. K. (2015). Expression of the astrocyte water channel aquaporin-4 in the mouse brain. *ASN Neuro* 7:1759091415605486. doi: 10.1177/1759091415605486
- Illarionova, N. B., Gunnarson, E., Li, Y., Brismar, H., Bondar, A., Zelenina, S., et al. (2010). Functional and molecular interactions between aquaporins and Na,K-ATPase. *Neuroscience* 168, 915–925. doi: 10.1016/j.neuroscience.2009.11.062
- Inoue, H., Mori, S., Morishima, S., and Okada, Y. (2005). Volume-sensitive chloride channels in mouse cortical neurons: characterization and role in volume regulation. *Eur. J. Neurosci.* 21, 1648–1658. doi: 10.1111/j.1460-9568.2005.04006.x
- Jayakumar, A. R., and Norenberg, M. D. (2010). The Na-K-Cl Co-transporter in astrocyte swelling. *Metab. Brain Dis.* 25, 31–38. doi: 10.1007/s11011-010-9180-3
- Jo, A. O., Ryskamp, D. A., Phuong, T. T., Verkman, A. S., Yarishkin, O., MacAulay, N., et al. (2015). TRPV4 and AQP4 channels synergistically regulate cell volume and calcium homeostasis in retinal müller glia. *J. Neurosci.* 35, 13525–13537. doi: 10.1523/JNEUROSCI.1987-15.2015
- Kang, J., Kang, N., Yu, Y., Zhang, J., Petersen, N., Tian, G. F., et al. (2010). Sulforhodamine 101 induces long-term potentiation of intrinsic excitability and synaptic efficacy in hippocampal CA1 pyramidal neurons. *Neuroscience* 169, 1601–1609. doi: 10.1016/j.neuroscience.2010.06.020
- Katada, R., Akdemir, G., Asavapanumas, N., Ratelade, J., Zhang, H., and Verkman, A. S. (2014). Greatly improved survival and neuroprotection in aquaporin-4-knockout mice following global cerebral ischemia. *FASEB J.* 28, 705–714. doi: 10.1096/fj.13-231274
- Kilb, W., Dierkes, P. W., Syková, E., Vargová, L., and Luhmann, H. J. (2006). Hypoosmolar conditions reduce extracellular volume fraction and enhance epileptiform activity in the CA3 region of the immature rat hippocampus. *J. Neurosci. Res.* 84, 119–129. doi: 10.1002/jnr.20871
- Kimelberg, H. K. (1995). Current concepts of brain edema. Review of laboratory investigations. *J. Neurosurg.* 83, 1051–1059. doi: 10.3171/jns.1995.83.6.1051
- Kimelberg, H. K. (2004). Increased release of excitatory amino acids by the actions of ATP and peroxynitrite on volume-regulated anion channels (VRACs) in astrocytes. *Neurochem. Int.* 45, 511–519. doi: 10.1016/j.neuint.2003.11.002
- Kimelberg, H. K. (2005). Astrocytic swelling in cerebral ischemia as a possible cause of injury and target for therapy. *Glia* 50, 389–397. doi: 10.1002/glia.20174
- Kimelberg, H. K., Macvicar, B. A., and Sontheimer, H. (2006). Anion channels in astrocytes: biophysics, pharmacology, and function. *Glia* 54, 747–757. doi: 10.1002/glia.20423
- Lauderdale, K., Murphy, T., Tung, T., Davila, D., Binder, D. K., and Fiacco, T. A. (2015). Osmotic edema rapidly increases neuronal excitability through activation of NMDA receptor-dependent slow inward currents in juvenile and adult hippocampus. *ASN Neuro* 7:1759091415605115. doi: 10.1177/1759091415605115
- Liang, D., Bhatta, S., Gerzanich, V., and Simard, J. M. (2007). Cytotoxic edema: mechanisms of pathological cell swelling. *Neurosurg. Focus* 22:E2. doi: 10.3171/foc.2007.22.5.3
- Lohr, J. W., and Grantham, J. J. (1986). Isovolumetric regulation of isolated S₂ proximal tubules in anisotonic media. *J. Clin. Invest.* 78, 1165–1172. doi: 10.1172/jci112698
- Lohr, J. W., and Yohe, L. (2000). Isovolumetric regulation of rat glial cells during development and correction of hypo-osmolality. *Neurosci. Lett.* 286, 5–8. doi: 10.1016/s0304-3940(00)01098-3
- Ma, T., Yang, B., Gillespie, A., Carlson, E. J., Epstein, C. J., and Verkman, A. S. (1997). Generation and phenotype of a transgenic knockout mouse lacking the mercurial-insensitive water channel aquaporin-4. *J. Clin. Invest.* 100, 957–962. doi: 10.1172/jci231
- MacAulay, N., and Zeuthen, T. (2012). Glial K⁺ clearance and cell swelling: key roles for cotransporters and pumps. *Neurochem. Res.* 37, 2299–2309. doi: 10.1007/s11064-012-0731-3
- MacVicar, B. A., Feighan, D., Brown, A., and Ransom, B. (2002). Intrinsic optical signals in the rat optic nerve: role for K⁺ uptake via NKCC1 and swelling of astrocytes. *Glia* 37, 114–123. doi: 10.1002/glia.10023
- Mola, M. G., Sparaneo, A., Gargano, C. D., Spray, D. C., Svelto, M., Frigeri, A., et al. (2016). The speed of swelling kinetics modulates cell volume regulation and calcium signaling in astrocytes: a different point of view on the role of aquaporins. *Glia* 64, 139–154. doi: 10.1002/glia.22921
- Nagelhus, E. A., Mathiesen, T. M., and Ottersen, O. P. (2004). Aquaporin-4 in the central nervous system: cellular and subcellular distribution and coexpression with KIR4.1. *Neuroscience* 129, 905–913. doi: 10.1016/j.neuroscience.2004.08.053
- Nielsen, S., Nagelhus, E. A., Amiry-Moghaddam, M., Bourque, C., Agre, P., and Ottersen, O. P. (1997). Specialized membrane domains for water transport in glial cells: high-resolution immunogold cytochemistry of aquaporin-4 in rat brain. *J. Neurosci.* 17, 171–180.

- Papadopoulos, M. C., Manley, G. T., Krishna, S., and Verkman, A. S. (2004). Aquaporin-4 facilitates reabsorption of excess fluid in vasogenic brain edema. *FASEB J.* 18, 1291–1293. doi: 10.1096/fj.04-1723fj
- Papadopoulos, M. C., and Verkman, A. S. (2013). Aquaporin water channels in the nervous system. *Nat. Rev. Neurosci.* 14, 265–277. doi: 10.1038/nrn3468
- Pasantes-Morales, H., and Tuz, K. (2006). Volume changes in neurons: hyperexcitability and neuronal death. *Contrib. Nephrol.* 152, 221–240. doi: 10.1159/000096326
- Rasmussen, R., Nedergaard, M., and Petersen, N. C. (2016). Sulforhodamine 101, a widely used astrocyte marker, can induce cortical seizure-like activity at concentrations commonly used. *Sci. Rep.* 6:30433. doi: 10.1038/srep30433
- Risher, W. C., Andrew, R. D., and Kirov, S. A. (2009). Real-time passive volume responses of astrocytes to acute osmotic and ischemic stress in cortical slices and *in vivo* revealed by two-photon microscopy. *Glia* 57, 207–221. doi: 10.1002/glia.20747
- Risher, W. C., Croom, D., and Kirov, S. A. (2012). Persistent astroglial swelling accompanies rapid reversible dendritic injury during stroke-induced spreading depolarizations. *Glia* 60, 1709–1720. doi: 10.1002/glia.22390
- Roper, S. N., Obenaus, A., and Dudek, F. E. (1992). Osmolality and nonsynaptic epileptiform bursts in rat CA1 and dentate gyrus. *Ann. Neurol.* 31, 81–85. doi: 10.1002/ana.410310115
- Rosen, A. S., and Andrew, R. D. (1990). Osmotic effects upon excitability in rat neocortical slices. *Neuroscience* 38, 579–590. doi: 10.1016/0306-4522(90)90052-6
- Rothman, S. M., and Olney, J. W. (1987). Excitotoxicity and the NMDA receptor. *Trends Neurosci.* 10, 299–302. doi: 10.1016/0166-2236(87)90177-9
- Rungta, R. L., Choi, H. B., Tyson, J. R., Malik, A., Dissing-Olesen, L., Lin, P. J., et al. (2015). The cellular mechanisms of neuronal swelling underlying cytotoxic edema. *Cell* 161, 610–621. doi: 10.1016/j.cell.2015.03.029
- Schindelin, J., Arganda-Carreras, I., Frise, E., Kaynig, V., Longair, M., Pietzsch, T., et al. (2012). Fiji: an open-source platform for biological-image analysis. *Nat. Methods* 9, 676–682. doi: 10.1038/nmeth.2019
- Schnell, C., Hagos, Y., and Hülsmann, S. (2012). Active sulforhodamine 101 uptake into hippocampal astrocytes. *PLoS One* 7:e49398. doi: 10.1371/journal.pone.0049398
- Schnell, C., Shahmoradi, A., Wichert, S. P., Mayerl, S., Hagos, Y., Heuer, H., et al. (2015). The multispecific thyroid hormone transporter OATP1C1 mediates cell-specific sulforhodamine 101-labeling of hippocampal astrocytes. *Brain Struct. Funct.* 220, 193–203. doi: 10.1007/s00429-013-0645-0
- Schwartzkroin, P. A., Baraban, S. C., and Hochman, D. W. (1998). Osmolarity, ionic flux, and changes in brain excitability. *Epilepsy Res.* 32, 275–285. doi: 10.1016/s0920-1211(98)00058-8
- Somjen, G. G. (1999). Low external NaCl concentration and low osmolarity enhance voltage-gated Ca currents but depress K currents in freshly isolated rat hippocampal neurons. *Brain Res.* 851, 189–197. doi: 10.1016/s0006-8993(99)02185-x
- Song, Y., and Gunnarson, E. (2012). Potassium dependent regulation of astrocyte water permeability is mediated by cAMP signaling. *PLoS One* 7:e34936. doi: 10.1371/journal.pone.0034936
- Strohschein, S., Hüttmann, K., Gabriel, S., Binder, D. K., Heinemann, U., and Steinhäuser, C. (2011). Impact of aquaporin-4 channels on K⁺ buffering and gap junction coupling in the hippocampus. *Glia* 59, 973–980. doi: 10.1002/glia.21169
- Su, G., Kintner, D. B., Flagella, M., Shull, G. E., and Sun, D. (2002a). Astrocytes from Na⁺-K⁺-Cl⁻ cotransporter-null mice exhibit absence of swelling and decrease in EAA release. *Am. J. Physiol. Cell Physiol.* 282, C1147–C1160. doi: 10.1152/ajpcell.00538.2001
- Su, G., Kintner, D. B., and Sun, D. (2002b). Contribution of Na⁺-K⁺-Cl⁻ cotransporter to high-[K⁺]_o-induced swelling and EAA release in astrocytes. *Am. J. Physiol. Cell Physiol.* 282, C1136–C1146. doi: 10.1152/ajpcell.00478.2001
- Sun, M. Y., Devaraju, P., Xie, A. X., Holman, I., Samones, E., Murphy, T. R., et al. (2014). Astrocyte calcium microdomains are inhibited by bafilomycin A1 and cannot be replicated by low-level Schaffer collateral stimulation *in situ*. *Cell Calcium* 55, 1–16. doi: 10.1016/j.ceca.2013.10.004
- Thrane, A. S., Rappold, P. M., Fujita, T., Torres, A., Bekar, L. K., Takano, T., et al. (2011). Critical role of aquaporin-4 (AQP4) in astrocytic Ca²⁺ signaling events elicited by cerebral edema. *Proc. Natl. Acad. Sci. U S A* 108, 846–851. doi: 10.1073/pnas.1015217108
- Tuz, K., Ordaz, B., Vaca, L., Quesada, O., and Pasantes-Morales, H. (2001). Isovolumetric regulation mechanisms in cultured cerebellar granule neurons. *J. Neurochem.* 79, 143–151. doi: 10.1046/j.1471-4159.2001.00546.x
- Wetherington, J., Serrano, G., and Dingledine, R. (2008). Astrocytes in the epileptic brain. *Neuron* 58, 168–178. doi: 10.1016/j.neuron.2008.04.002
- Wurm, A., Lipp, S., Pannicke, T., Linnertz, R., Krügel, U., Schulz, A., et al. (2010). Endogenous purinergic signaling is required for osmotic volume regulation of retinal glial cells. *J. Neurochem.* 112, 1261–1272. doi: 10.1111/j.1471-4159.2009.06541.x
- Xie, A. X., Lauderdale, K., Murphy, T., Myers, T. L., and Fiocco, T. A. (2014). Inducing plasticity of astrocytic receptors by manipulation of neuronal firing rates. *J. Vis. Exp.* 85:e51458. doi: 10.3791/51458
- Yan, Y., Dempsey, R. J., Flemmer, A., Forbush, B., and Sun, D. (2003). Inhibition of Na⁺-K⁺-Cl⁻ cotransporter during focal cerebral ischemia decreases edema and neuronal damage. *Brain Res.* 961, 22–31. doi: 10.1016/s0006-8993(02)03832-5
- Yao, X., Hrabětová, S., Nicholson, C., and Manley, G. T. (2008). Aquaporin-4-deficient mice have increased extracellular space without tortuosity change. *J. Neurosci.* 28, 5460–5464. doi: 10.1523/JNEUROSCI.0257-08.2008
- Zhou, N., Gordon, G. R., Feighan, D., and MacVicar, B. A. (2010). Transient swelling, acidification, and mitochondrial depolarization occurs in neurons but not astrocytes during spreading depression. *Cereb. Cortex* 20, 2614–2624. doi: 10.1093/cercor/bhq018

Conflict of Interest Statement: The authors declare that the research was conducted in the absence of any commercial or financial relationships that could be construed as a potential conflict of interest.

Copyright © 2017 Murphy, Davila, Cuvelier, Young, Lauderdale, Binder and Fiocco. This is an open-access article distributed under the terms of the Creative Commons Attribution License (CC BY). The use, distribution or reproduction in other forums is permitted, provided the original author(s) or licensor are credited and that the original publication in this journal is cited, in accordance with accepted academic practice. No use, distribution or reproduction is permitted which does not comply with these terms.